Aus dem Institut für Integrative Neuroanatomie
der Medizinischen Fakultät Charité – Universitätsmedizin Berlin

DISSERTATION

Electrophysiological and Morphological Characteristics of VGAT-YFP positive Neurons in the Lateral Habenula of the Rat

zur Erlangung des akademischen Grades
Doctor medicinae (Dr. med.)

vorgelegt der Medizinischen Fakultät
Charité – Universitätsmedizin Berlin

von
Leo Fabig

aus Hamburg

Datum der Promotion: 17.09.2021

Table of Content / Inhaltsverzeichnis

Image Index / Abbildungsverzeichnis

1 Abbreviations

%	percentage
ADP	afterdepolarizing potential
AHP	afterhyperpolarization
AMPA	α-amino-3-hydroxy-5-methyl-4-isoxazolepropionic acid
AP	action potential
CAN	Ca^{2+}-activated non-selective cation channel
CB	calbindin
CC	current clamp
DNQX	6,7-dinitroquinoxaline-2,3-dione
EPSC	excitatory postsynaptic current
fr	*fasciculus retroflexus*
GABA	*gamma*-aminobutyric acid
GAD67	glutamate acid decarboxylase isotype 67
Hb	habenula
IPSC	inhibitory postsynaptic current
ISI	interspike interval
Hz	hertz
kD	kilodalton
kHz	kilohertz
LHb	lateral habenula

MHb	medial habenula
ms	milliseconds
nA	nanoampere
NGS	normal goat serum
pA	picoampere
PB	phosphate buffer
PBS	phosphate saline buffer
PPR	paired pulse ratio
PV	parvalbumin
PVP	posterior paraventricular thalamic nucleus
RMTg	rostromedial tegmental nucleus
RNA	ribonucleic acid
R_{IN}	input resistance
R_S	series resistance
RT	room temperature
sm	*stria medullaris*
SNpc	substantia nigra pars compacta
VC	voltage clamp
VGAT	vesicular *gamma*-aminobutyric acid transporter
VTA	ventral tegmental area
YFP	yellow fluorescent protein

2 Abstract

2.1 Abstract

In recent years, research on the cellular basis of neuropsychiatric disorders has increasingly focused on the lateral habenula (LHb) as a crucial structure for the understanding of depression. The LHb is a phylogenetically old structure located in the diencephalon and connects limbic forebrain structures with monoaminergic centers in the midbrain and brainstem, thereby playing an important role in reward-based behavior. Convergently, chronic hyperactivity of LHb neurons has been found in animal models of depression.

The LHb is widely regarded as a simple relay station and despite growing interest over the last two decades, little is known about the connectivity and processing of information within this brain area. In the neocortex and the hippocampus, GABAergic interneurons are well known to orchestrate the local flow of information. To identify potential inhibitory interneurons within the LHb, whole-cell patch clamp recordings were performed in brain slices of transgenic rats. In these rats, certain neurons express the yellow fluorescent protein (YFP) Venus under the control of the VGAT promoter, which is known to be abundantly expressed in cortical GABAergic interneurons.

YFP-positive neurons were found in low numbers, preferentially located in the medial part of the caudal LHb. However, results of *in situ* hybridization showed that they were negative for the GABA synthesizing enzyme isoform GAD-67, and morphological analyses did not show morphological features of interneurons such as an extensively branching local axon. Nevertheless, they differed from YFP-negative LHb neurons in terms of firing pattern and passive electrophysiological properties, as well as the trajectory of the axon. Interestingly, a group of YFP-positive cells additionally showed an extensively branching dendritic tuft extending into the neighboring posterior paraventricular nucleus of the thalamus. This indicates a direct functional link between the thalamus and LHb, two brain regions that were thought to be anatomically and functionally segregated. To further elucidate the inputs to single YFP-positive LHb neurons, extracellular electrical stimulation of the *stria medullaris* (a major fiber tract conveying input from the forebrain to the LHb) and the paraventricular thalamus was performed. Noting experimental limitations, the results suggest that the input to YFP-positive cells is both glutamatergic and GABAergic.

In summary, YFP-positive neurons form a distinct entity of cells in the LHb and exhibit features of projection neurons, rather than inhibitory interneurons. The precise identity of these cells, as well as the functional relevance of their connection to the thalamus remain to be elucidated.

2.2 Zusammenfassung

Die laterale Habenula (LHb) und ihre Verbindungen spielen eine herausragende Rolle im heutigen Verständnis von Belohnungsverhalten und der Entstehung neuropsychiatrischer Erkrankungen wie der Depression. Die LHb ist eine phylogenetisch alte Hirnregion des Diencephalons und verbindet limbische Strukturen des Vorderhirns mit monoaminergen Zentren in Mittelhirn und Hirnstamm.

Diese Funktion als einfache Relaisstation bestimmt auch heute das Verständnis der LHb und trotz intensiver Forschung innerhalb der letzten 20 Jahre ist über die Verschaltung und die Informationsverarbeitung innerhalb der LHb noch immer wenig bekannt. In Neokortex und Hippocampus steuern GABAerge Interneurone den Informationsfluss. Mithilfe der transgenen VGAT-Venus-A-Ratte und der Whole-Cell Patch clamp-Technik untersuchten wir deshalb die Eigenschaften einer Untergruppe von Neuronen in der LHb und ihre mögliche Funktion als inhibitorische Interneurone. Diese Zellen exprimieren das gelb fluoreszierende Protein Venus (YFP-positive Zellen) unter dem VGAT-Promoter, der stark in kortikalen GABAergen Interneuronen exprimiert wird.

Die untersuchten YFP-positiven Zellen fanden sich in geringer Anzahl, vor allem im medialen Teil der kaudalen LHb. Sie waren negativ für die Isoform des GABA-synthetisierenden Enzyms GAD-67 und wiesen in der morphologischen Analyse kein stark verzweigtes, lokales Axon auf, wie es für kortikale Interneurone typisch ist. Jedoch fanden sich deutliche Unterschiede zu den YFP-negativen Zellen in der LHb hinsichtlich des Feuermusters, passiver elektrophysiologischer Eigenschaften und des Verlaufs des Axons. Interessanterweise reichte der basale, stark verzweigte Dendrit einer Gruppe von YFP-positiven Zellen in den benachbarten posterioren paraventrikulären Thalamus und bildete so eine direkte funktionelle Verbindung zwischen zwei Hirnregionen, die zuvor sowohl anatomisch als auch funktionell als getrennt betrachtet wurden.

Mithilfe extrazellulärer, elektrischer Stimulation der s*tria medullaris*, welche die Afferenzen der LHb aus dem Vorderhirn führt, und des benachbarten paraventrikulären

Thalamus konnten wir außerdem zeigen, dass, unter Berücksichtigung der kleinen Fallzahl, YFP-positive Zellen sowohl glutamaterg als auch GABAerg innerviert sind.
Zusammenfassend zeigten die untersuchten YFP-positiven Neurone keine typischen Merkmale inhibitorischer Interneurone, unterschieden sich jedoch deutlich von den YFP-negativen Zellen der LHb. Die genaue Identität dieser Zellen und die funktionelle Relevanz ihrer Verbindung zum Thalamus bleiben zu untersuchen.

3 Introduction

3.1 In the center of the brain

On a gross paramedian section of the brain, the habenula is barely noticeable. But directing the view to the center, one can notice a small structure bordered superiorly by the ventricles. Nearby, at the pineal gland, Descartes hypothesized the seat of the human soul (Fig. 1). Albeit scientific interest soon shifted outwards to the cortical regions of the brain, in recent years the habenula has attracted considerable attention due to its influence on monoaminergic centers in the brainstem and its role in reward behavior, as well as neuropsychiatric disorders (Hikosaka 2010).

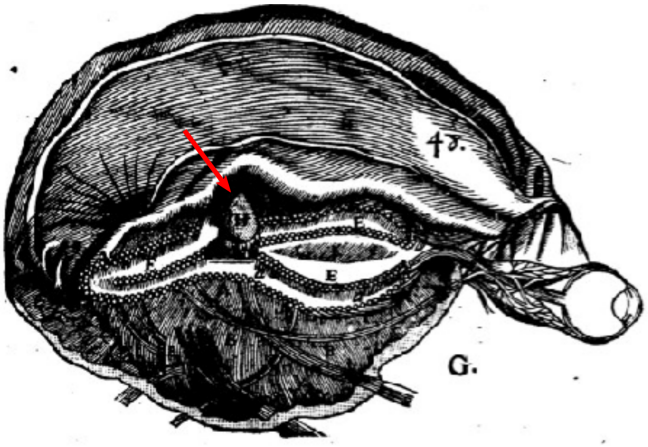

Figure 1: The pineal gland in a drawing by Descartes.
The pineal gland (H, red arrow) is depicted in the center of a human brain, suspended among the ventricles (Descartes, R., 1664).

The habenula helps to regulate the levels of serotonin and dopamine in the brain. These two neurotransmitters are of paramount importance in cognitive functioning. Dopamine, for example, has been shown to play an important role in locomotion, motivational control and reward-based learning (Bromberg-martin, Matsumoto, and Hikosaka 2010). Reward can be conceptualized as a positive value that is assigned to an object, act or stimulus and provides an explanatory framework for the conditioning experiments of Pavlov in the 1920s. Reward-based learning helps animals and humans to predict the future based on prior experiences and this anticipation is critical for decision making in complex environments. In the 1990s Schultz and colleagues identified the dopaminergic neurons in the ventral tegmental area (VTA) as an important component of the reward system (Schultz, Dayan, and Montague 1997). In a seminal study, Matsumoto and Hikosaka demonstrated the importance of the lateral habenula in reward processing. Macaque monkeys were subjected to a visually guided saccade task while simultaneously recording the activity of neurons in the VTA and the lateral habenula. They showed that habenula neurons vary in their firing frequency in response to both delivery and omission

of a reward and that these neurons exert a strong influence on the dopaminergic cells in the VTA (Matsumoto and Hikosaka 2007).

Also, serotonin has been linked to reward-based learning, but on a larger time scale (Bromberg-martin, Hikosaka, and Nakamura 2010; Cohen, Amoroso, and Uchida 2015). Serotoninergic neurons in the raphe nuclei of the brainstem project throughout the brain and serotonin acts on a multitude of different receptor subtypes, such as the ionotropic 5-HT_3-receptor and various G-protein coupled receptors. These neurons were shown to participate in the control of mood states and sleeping cycles (Monti 2011).
The LHb and the raphe nuclei are mutually connected and increased activity of the LHb reduces the firing rate of serotonergic neurons in the raphe nuclei and vice versa. In an animal model of depression, optogenetic stimulation of the fibers from the dorsal raphe to the LHb was shown to alleviate depressive-like behavior in rats (H. Zhang et al. 2018).

Lesions of the habenular complex result in manifold behavioral alterations, such as attention and learning deficits (Lecourtier and Kelly 2007). Given the important role of the lateral habenula in reward-based learning further questions arise about its contribution to neuropsychiatric disorders, such as drug addiction and depression.

3.2 The habenula in depression

The LHb appears to be a major node in the network responsible for depression. If one follows the monoamine hypothesis of depression, chronic hyperactivity of the LHb, and the resulting depletion of dopamine and serotonin in other brain areas, could at least partially account for typical symptoms of depression (Boku et al. 2018; Yang, Wang, et al. 2018). These include the inability to feel pleasure (anhedonia), reduced motivational drive and motoric hypoactivity. In recent years important insights were gained in the cellular and molecular mechanisms of depressive states. Increased burst firing activity of neurons in the LHb was observed in rats with learned helplessness, an animal model of depression. This was caused by synaptic potentiation, i.e., more effective synaptic transmission of afferent projections from the forebrain and basal ganglia, due to increased membrane trafficking of glutamatergic AMPA receptors mediated by an upregulation of a calcium kinase (ßCaMKII). The hyperactivity could be reversed by both deep brain stimulation in the LHb and by antidepressant treatment with imipramine (Li et al. 2011,

2013). Furthermore, ketamine, a pharmacologic agent that is used for treatment of refractory depression, was shown to work by blocking the burst response of neurons in the LHb (Yang, Cui, et al. 2018). Finally, a recent study demonstrated a multisynaptic connection of neurons in the retina to the LHb via the lateral geniculate nucleus of the thalamus, and photostimulation of this pathway resulted in decreased depressive behavior in a mouse model (Huang et al. 2019).

These insights not only help us to better understand the mechanism responsible for the effect of antidepressant drugs but might also aid in guiding therapy by brain stimulation. This was successfully tried in one patient with major depressive disorder refractory to other treatment options (Sartorius et al. 2010).

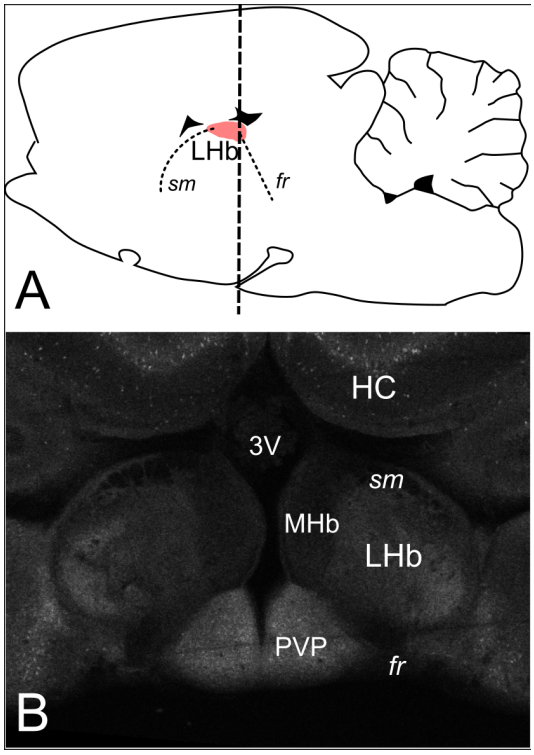

Figure 2: Anatomy of the habenula.

A: Schematic representation of a sagittal section through a rat brain at –3.6 mm from Bregma. The vertical bar represents the section shown in panel B.

B: Coronal section showing the habenula in the VGAT-Venus-A rat.

Abbreviations: 3V - third ventricle; *fr* - *fasciculus retroflexus*; HC - hippocampus; LHb - lateral habenula; PVP - posterior paraventricular thalamus; *sm* - *stria medullaris.*

3.3 Anatomy of the habenula

The habenula is a phylogenetically old structure, well conserved across species, and present in mammals, as well as fish, reptiles and birds (Aizawa, Amo, and Okamoto 2011). Together with the pineal gland, the habenula forms the epithalamus, and is located caudally on the dorsal aspect of the thalamus, adjacent to the ventricles. It can be subdivided into a smaller medial part (MHb) and a larger lateral one (LHb) (Fig. 2B).

The LHb can be further divided into several nuclei by taking into account the cell density and shape, as well as the immunoreactivity against diverse neuronal markers such as tyrosine hydroxylase and GABA-B receptor (Aizawa et al. 2012; Bernard and Veh 2012).

3.4 Connectivity of the habenula

The habenula is a relay station that allows reciprocal control and communication between limbic forebrain structures and monoaminergic centers in the brainstem. In the stria

medullaris (*sm*), inputs from limbic forebrain structures and the basal ganglia reach the habenular nuclei. The vast majority of this input is excitatory, depolarizing habenular neurons via ionotropic glutamatergic AMPA-Receptors (Shabel et al. 2012). The output, on the other hand, leaves the habenula through the *fasciculus retroflexus* (*fr).* Distinct parts of the habenula target specific regions in the brainstem (Fig. 3). The MHb mainly targets the interpeduncular nucleus, whereas the targets of the LHb are more widespread. The most prominent and best reviewed targets of the lateral part of the LHb are GABAergic cells in both the ventral tegmental area and the mesopontine rostromedial tegmental nucleus (also called “tail” of the VTA). These neurons inhibit the dopaminergic neurons of the VTA and the substantia nigra pars compacta (SNpc) (Gonçalves, Sego, and Metzger 2012; Jhou et al. 2009), and thereby exert a strong control over the dopamine levels in both the striatum and the prefrontal cortex.

The preferential targets of neurons in the medial part of the LHb are the median and paramedian raphe nuclei and the dorsal raphe nucleus (Bernard and Veh 2012; Kim 2009). These nuclei provide serotoninergic input to the telencephalon and to the spinal cord. The LHb neurons primarily target inhibitory interneurons in the raphe nuclei, and thus seem to inhibit serotoninergic transmission (Varga, Kocsis, and Sharp 2003).

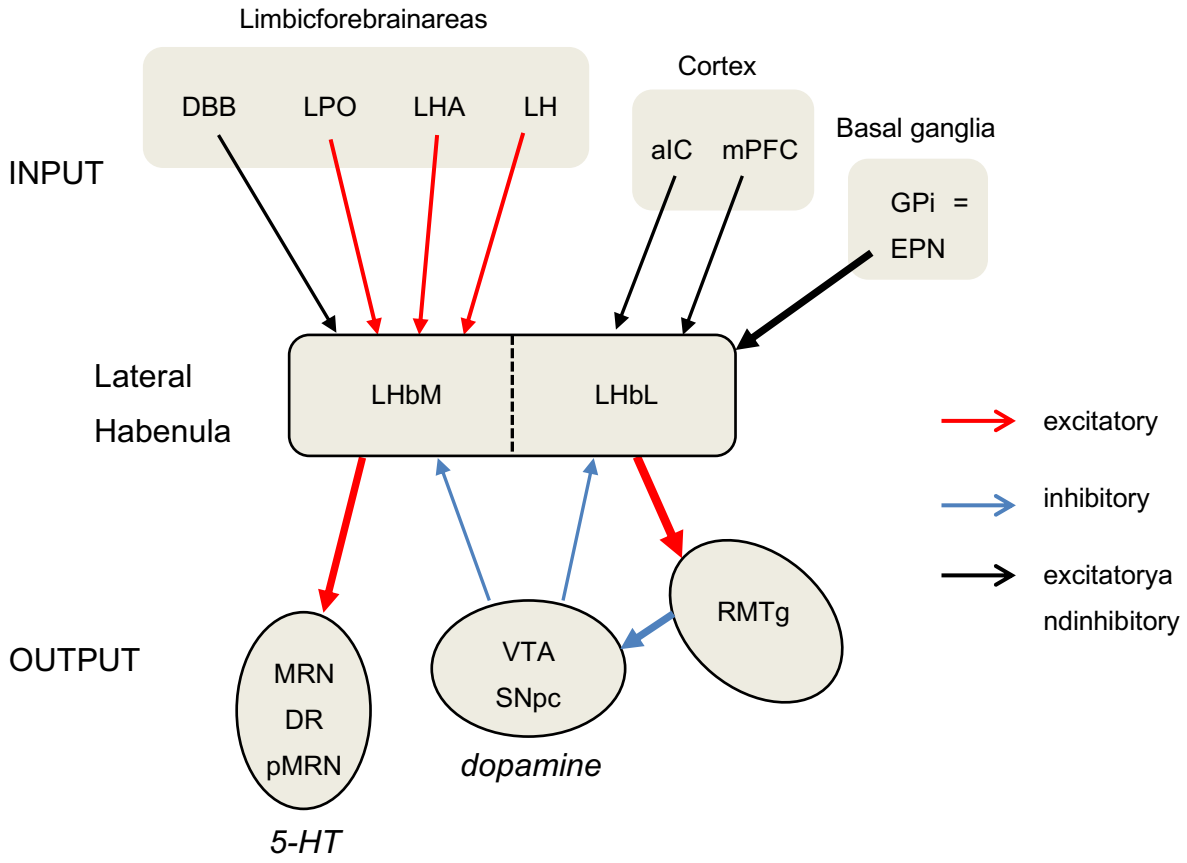

Figure 3: Schematic representation of the connections of the lateral habenula (LHb).

The lateral part of the LHb receives input from the basal ganglia and the cortex and controls primarily dopaminergic systems in the brainstem (VTA and SNpc). The medial part of the LHb is mainly innervated by lateral hypothalamic nuclei and directly influences serotoninergic systems i.e. the raphe nuclei. The strength of the arrows represents the density of connections between respective areas.

Abbreviations: aIC - anterior internal capsule; DBB - diagonal band of Broca; DR - dordal raphe; EPN: - entopeduncular nucleus; GPi - globus pallidus internal segment; LHbM - medial part of lateral habenula; LHbL - lateral part of lateral habenula; LH - lateral hypothalamus, LHA - lateral hypothalamic area; LPO - lateral preoptic nucleus; MnR - median raphe nucleus, pMnR - paramedian raphe nucleus; RMTg - rostromedial tegmental nucleus; SNpc - substantia nigra pars compacta; VTA - ventral tegmental area.

Adapted and modified from: (Proulx, Hikosaka and Malinow, 2014).

3.5 Morphological and electrophysiological characteristics of neurons in the lateral habenula

Neurons in the LHb have small, round to oval cell bodies and 2-4 dendrites (Weiss and Veh 2011) (Fig. 4). The axons typically follow a lateral to latero-ventral direction and enter the *fasciculus retroflexus* with or without minimal branching within the LHb, though they display swellings suggestive of en-passant boutons on their way (Kim and Chang 2005).

Based on their firing pattern at resting membrane potential, the neurons can be divided into three physiological groups: tonic firing, silent and burst oscillating cells (Kim and Chang 2005). LHb neurons are electrophysiologically compact with high input resistances.

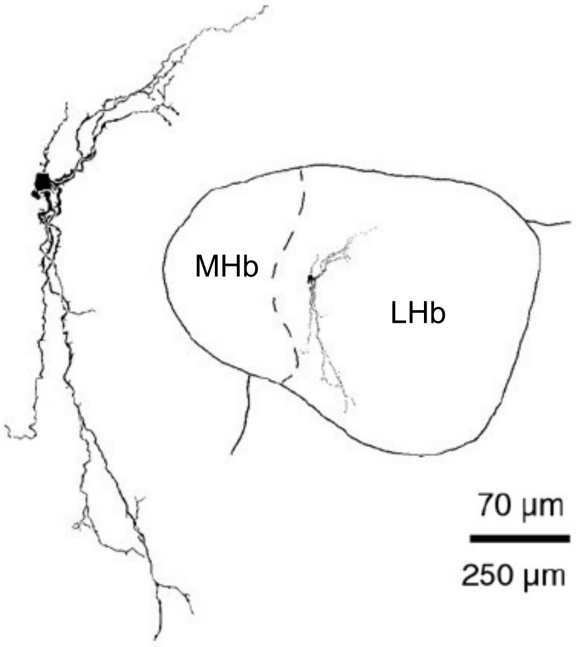

Figure 4: Camera lucida drawing of a neuron in the lateral habenula.

Note the vertical orientation and small, round cell body. Reproduced from: (Weiss and Veh 2011).

Abbreviations: MHb – medial habenula; LHb – lateral habenula.

A remarkable feature of most LHb neurons is their ability to elicit a burst response following a short hyperpolarizing current pulse. This bursting is usually followed by a long-lasting train of action potentials. While the burst response relies mainly on L-Type calcium channels, the subsequent influx of calcium triggers the opening of calcium-activated non-selective cation channels (CANs), which leads to a sustained depolarization (Chang and Kim 2004). There seems to be no relationship between morphological and electrophysiological characteristics. Physiological variables such as firing pattern, and morphological parameters, such as the primary orientation of the dendrites or their position in the LHb, were found to be unrelated in LHb neurons (Weiss and Veh 2011).

3.6 Intrahabenular connectivity and interneurons?

The lateral habenula is largely seen as a relay station for parallel, separate streams of information that only allow for the regulation of the effectiveness of transmission. This

view is supported by the very low number of labeled and presumably GABAergic cells with a potential function as inhibitory interneurons in the LHb observed in studies using *in situ* hybridization against GAD67-RNA (Brinschwitz et al. 2010). In fact, the glutamatergic input to the LHb seems to be balanced by co-release of GABA, and not by specialized inhibitory cells (Shabel et al. 2014). This view has been challenged by recent experimental data showing a small number of GABAergic cells in the medial part of the LHb with an axon that shows local arborization (L. Zhang et al. 2018; Zhang and Hernández 2016). In summary, to date there has been little research regarding the local network processing of information within the LHb, such as convergence and divergence of inputs, or connectivity within the LHb.

In our research group, the VGAT-Venus-A-rat has become an indispensable tool to study interneuron morphology and function in cortical areas, such as the hippocampus. The VGAT-Venus-A rat is a transgenic animal expressing the yellow fluorescent protein (YFP) Venus under the control of the VGAT promoter (Uematsu et al. 2008). VGAT (vesicular *gamma*-aminobutyric acid transporter) ensures the traffic of GABA into vesicles and is therefore expressed selectively in GABAergic neurons. While the labeling of GABAergic neurons in cortical areas is accurate, prominent mis-expression has been reported in the thalamus (Uematsu et al. 2008).

3.7 Aims of the study

- What are the electrophysiological and morphological properties of Venus-expressing neurons in the LHb, and what neuronal markers do they express?
- Do Venus-expressing cells in the LHb form a homogenous population, or can they be subdivided into different groups?
- Are Venus-expressing cells in the LHb different from the glutamatergic projection neurons of the LHb characterized previously (Weiss and Veh 2011).
- Are Venus-expressing cells in the LHb GABAergic, and can they be assigned a potential role as inhibitory interneurons with local connectivity?

4 Materials and Methods

4.1 Materials

4.1.1 Devices

Table 1: List of devices used in this study

Device / Material	**Name**	**Company**
Microscope for patching	U-Tluir with XLUM PlanTLN objective (x20 / 1.00 W)	Olympus
Working stage and micromanipulator	PatchStar	Scientifica
Digital camera	Retiga 2000R	Q Imaging
Amplifier for patch clamp	Multiclamp 700B	Axon (Millipore)
Headstage	CV-7B	Axon (Millipore)
Pipette puller	P-97	Sutter Instruments Co.
Borosilicate glass tubing		Kwik-Fil
Extracellular stimulator	DS2A-Mk.II	Digitimer Ltd.
Fluorescence lamp	pE-100	CoolLED
Light-source	SS 3200-00	Scientifica
Oscilloscope	TDS 1001C-EPU	Tektronix
Analogue-to-digital converter	NI USB-6259	National Instruments
Vibratome	VT1200s;	Leica
Constant Voltage Stimulator	DS2A-Mk.II	Digitimer Ltd.
Heater	TMP-5b	Supertech

Pressure monitor	PRM-3a	Supertech
Pump	Minipuls 3	Gilson
Confocal microscope	FV1000	Olympus
Objective (x20) for confocal	UPlanSApo 20x/0.75	Olympus
Fluorescence microscope	Axiovision 4.8 5x/XXX, 20x/XXX	Zeiss

4.1.2 Software

Table 2: List of software used for data procession and analysis

Software	**Company / Author**
WinWCP V4.5.2	John Dempster, University of Strathclyde
Stimfit 0.10	(Schlögl et al. 2013), www.stimfit.org
ImageJ	W.S. Rasband, National Institutes of Health, Bethesda, Maryland, http://rsb.info.nih.gov/ij/
Simple Neurite Tracer Plugin in ImageJ	Mark Longair (Longair, Baker, and Armstrong 2011)
SPSS Statistics 22	IBM
Fluoview V.4.06	Olympus
IrfanView	Irfan Skiljan, Austria
MicroManager Version 1.4	(Edelstein et al. 2010)

4.1.3 Chemicals

Table 3: List of chemicals used in experiments

Chemicals	**Specification / formula**	**Company**
Paraformaldehyde	CH_2O	Merck

Picric acid	2,4,6-trinitrophenol	
Biocytin	amide formed by biotin and L-lysine	Life Technologies
TrisHCl	tris(hydroxymethyl)aminomethane - hydrochloride	Roth
NaAzide	NaN_3	
Triton X-100	Nonionic surfactant	
Agar-Agar	Agarose and agaropectin polymer	
EGTA	ethylene glycol tetraacetic acid	Sigma-Aldrich
HEPES	4-(2-hydroxyethyl)-1-piperazineethanesulfonic acid	
Na_2ATP	Adenosine 5´-triphosphate disodium salt	
GTP xNa^+	Guanosine-5´-triphosphate sodium salt hydrate	

4.1.4 Pharmacological agents

Table 4: List of pharmacological agents used in experiments

Pharmacological agents	**Description**	**Company**
DNQX	AMPA-receptor antagonist	Abcam or Tocris
Gabazine	GABA-A and GABA-C receptor antagonist	

4.1.5 Buffers and solutions

Table 5: List of buffers and solutions used in experiments

Buffers and solutions	**Contains**

Phosphate buffer (PB)	0.1 M contains: 0.1 M Na_2HPO_4 titrated to pH 7.2 with 0.1 M NaH_2PO_4
Phosphate buffered saline (PBS)	1 M contains: 137 mM NaCl, 27 mM KCl, 10 mM Na_2HPO_4, 1.8 mM KH_2PO_4 and pH adjusted to 7.4
4% Paraformaldehyde (4% PA)	For 1 liter: 40 mg paraformaldehyde, 400 ml H_2O, 500 ml PB 0.2 M, drops of 1N NaOH to help dissolution of paraformaldehyde
Saline-sodium citrate (SSC)	20 x concentrated: 87.65 g NaCl, 44.1 g Na-citrate in 500ml, pH 7.0 – 7.2
Hybridisation buffer (HB)	50% Formamide, 4x SSC, 5% Dextran sulfate, 250 µg/ml heat-denaturated salmon sperm DNA, 100 µg/ml t-RNA, 1x Denhardt's solution
Denhardt's solution	1 % Ficoll, 1% polyvinylpyrrolidone, 1% bovine serum albumin
TBS pH 7.5	100 mMTris/HCl pH 7.5, 150 mM NaCl
1 % blocking solution	Dissolved in TBS pH 7.5
Substrate buffer	100 mMTris/HCl pH 9.5, 100 mM NaCl, 50 mM $MgCl_2$
Internal pipette solution	[mM] 130 K-gluconate, 10 KCl, 10 EGTA, 10 HEPES, 2 $MgCl_2$, 2 Na_2ATP, 0.3 Na_2GTP, 1 $Na_2Creatine$ with 0.1% biocytin
Artificial cerebrospinal fluid (ACSF)	[mM] 125 NaCl, 2.5 KCl, 25 $NaHCO_3$, 1.25 NaH2PO_4, 25 glucose, 1 pyruvate, 1 ascorbate, 2 $CaCl_2$, 1 $MgCl_2$
Sucrose solution for *invitro* slices (sucrose ACSF)	[mM] 87 NaCl, 2.5 KCl, 25 $NaHCO_3$, 1.25 NaH_2PO_4, 25 glucose, 75 sucrose, 1 pyruvate, 1 ascorbate, 0.5 $CaCl_2$, 7 $MgCl_2$,

4.1.6 Antibodies and dyes

Table 6: List of antibodies and dyes used in experiments

Antibodies, dyes and mounting media	**Description**	**Company**
Rabbit anti-parvalbumin	Polyclonal, primary antibody	Swant
Rabbit anti-calbindin	Polyclonal, primary antibody	Swant
Rabbit anti-B17	Polyclonal, primary antibody	Invitrogen
Rabbit anti-NeuN	Monoclonal, primary antibody	Millipore

Mouse anti-GFP	Polyclonal, primary antibody	Invitrogen
Rabbit anti-GABA	Polyclonal, primary antibody	ImmuSmol
Alexa Flour 488 goat anti-mouse	Polyclonal, secondary antibody	Invitrogen
Alexa Flour 546 goat anti-rabbit	Polyclonal, secondary antibody	Invitrogen
Alexa Flour 647 goat anti-rabbit	Polyclonal, secondary antibody	Invitrogen
Streptavidin, Alexa Flour 647 conjugate		Molecular Probes, Life Technologies
Sheep anti-Digoxigenin-AP, conjugated with alkaline phosphatase	F_{ab}-fragments from polyclonal antibodies	Roche
Normal goat serum (NGS)		Vector companies
Substrate solution (for alkaline phosphatase)	100 mg/ml nitro-blue tetrazolium chloride (NBT), 50 mg/ml 5-bromo-4-chloro-3'-indolyphosphate p-toluidine salt (BCIP)	
Fluorescent mounting medium	Anti-fade	Invitrogen
Aqueous mounting medium	Immu-mount	ThermoScientific

4.2 Methods

4.2.1 Electrophysiological recordings

Slice preparation: 18- to 25-day-old Wistar rats expressing the fluorescent protein Venus under the VGAT promoter (Uematsu et al. 2008) were decapitated rapidly in accordance with the National Guidelines. All experiments were approved by LaGeSo Berlin (T-0215/11).

The brain was then carefully removed from the skull and placed into ice-cold sucrose solution continually perfused with carbogen (95% O_2, 5% CO_2). Afterwards, both the rostral and the caudal quarter of the brain were removed by coronal cuts and using cyanoacrylate-based glue the brain was glued onto a platform for the slicing chamber,

with the resulting rostral cutting area. Conversely, sagittal slices were obtained by the same procedure using sagittal cuts. Coronal or sagittal slices of 300 µm thickness containing the habenular complex were then cut using a vibratome (VT1200s, Leica) in ice-cold sucrose solution. They were then transferred into a holding chamber containing sucrose solution and stored for 30 min at around 33 °C, bubbled continuously with carbogen. Afterwards, the slices were kept at room temperature close to the recording station. For recording, the slices were placed in a submerged recording chamber and superfused with carbogenated ACSF at 32-34 °C at a rate of 25 ml/min.

Some slices were not turned after slicing, to allow the patching of cells from the caudal aspect of the slice and the tracing of the axon if it traveled in the rostral direction.

Target cell identification: Using a microscope (BX-51, Olympus) and the Dodt-contrast method, the LHb could be identified easily due to its midline position bordered by the ventricles superiorly. The border towards the MHb was demarked clearly by the increased densities of cells; regarding the adjacent thalamic nuclei, the border was less obvious, but in general thalamic cells showed a bigger cell body, and the number of fluorescent cells was far higher. YFP+ cells were identified by the fluorescence signal and their identity was once more confirmed after breakthrough of the patched membrane (Fig. 5B).

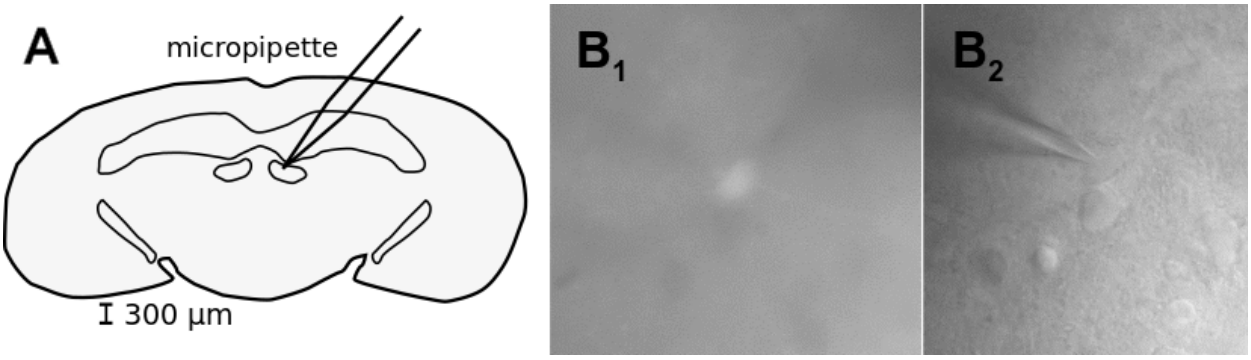

Figure 5: Scheme of patching process and target cell identification.

A: Diagram of coronal slice and patching pipette placed in habenular region.

B: VGAT-YFP-identity of the patched neuron confirmed by fluorescence microscopy (**B1:** epifluorescence; **B2:** infrared).

Whole-cell patch clamp Pipettes for recording were pulled from borosilicate glass capillaries (2 mm outer, 1 mm inner diameter, Hilgenberg) and filled with internal pipette solution (Tab. 6), containing 0.1% biocytin for subsequent visualization of recorded cells. The series resistance of the pipettes (R_S) was monitored constantly using a 5 mV test pulse, and ranged from 2-5 MΩ after filling them. Before moving the pipette into the bath,

a positive pressure of around 30 mbar was applied to prevent dust collecting on the tip of the pipette. When the surface of the slice was reached, this pressure was increased to 70-100 mbar to facilitate the movement of the pipette through the neuropil. Under visual control, the pipette was moved in close proximity to the cell body and the pressure rapidly lowered to 0 mbar in order to establish a stable seal. After the cell-attached mode was obtained, the seal resistance was calculated. If the seal resistance exceeded 3 GΩ, gentle suction was applied to break through the cell membrane and establish direct contact with the inside of the neuron. Series resistance (R_S) was determined at the beginning and end of the experiment, and recordings were discarded if R_S exceeded 25 MΩ. The resting membrane potential was recorded within one minute after breakthrough in current-clamp mode without current injection (I=0 mode of the amplifier). At the end of the experiment, the pipette was withdrawn carefully from the neuron to establish an outside-out patch.

The recordings were performed using an Axon Multiclamp 700B (Molecular Devices) amplifier. The signals were filtered at 5 kHz using the amplifier's built-in low-pass Bessel filter, and were digitized at 20 kHz (NI USB-6259; National Instruments) and stored for offline analysis using WinWCP software (V4.5.2, courtesy of John Dempster, University of Strathclyde). The recorded data was analyzed with the Stimfit software (Schlögl et al. 2013).

Recording of active and passive firing properties: After whole-cell patch clamp was established, the following protocols were run to determine the active and passive firing properties of the patched neuron. In current clamp (CC), bridge balance was used to allow for compensation of R_S. The signals were digitized at a rate of 10 KHz and filtered with a low pass Bessel filter at a 6 KHz cut-off frequency. The recording time of a trace was 1 second throughout.

(1) To analyze the basic firing behavior of the neuron and its input resistance, the membrane potential of the cell was adjusted to −65 mV by continuous bias current injection, and current pulses of 500 ms length were applied. The amplitudes of the current pulses started from −50 pA and increased in 50 pA steps until the action potential (AP) amplitude started to diminish markedly comparing the first and the last AP of a train. In the 200 pA stimulation trace, the interspike intervals (ISIs) were evaluated, as well as the firing frequency, and the amount of afterhyperpolarization (AHP) following a train of action potentials. The −50 pA stimulation trace was used to calculate the amount of delayed inward rectification (Sag-index).

(2) To assess the input resistance (R_{in}) of the cell, small hyperpolarizing current pulses (−5 pA or −2 pA in more compact cells) were applied repeatedly for 500 ms at a holding potential of −65 mV.

(3) To measure the membrane time constant (τ), a strong (−1 nA) but short (1ms) current pulse was applied repeatedly. If this pulse elicited a rebound burst response, the amplitude was reduced to −0.5 nA.

(4) To evaluate the firing behavior and action potential characteristics of the neuron, small current steps were used starting from three different membrane potentials (−55, −65, −75 mV). In the −55 mV trace, the current amplitudes usually ranged from −100 pA to +100 pA. The currents were increased stepwise by 5 to 10 pA.

(5) In voltage clamp (VC), at a holding potential of −65 mV, the response to a voltage step of −5 mV amplitude and 500 ms duration was measured. This allowed us to calculate the *membrane capacitance (C_M*; see below for equation).

Extracellular electrical stimulation: To apply extracellular stimulation, glass pipettes used for patching (see above) were filled with ACSF or 2 M sodium chloride and positioned in the *stria medullaris* or the paraventricular posterior thalamic nuclei (PVP), 100 - 300 µm away from the cell body. A constant voltage stimulator (Digitimer Ltd. DS2A-Mk.II unit) was used for extracellular stimulation with amplitudes from 10 to 50 V and a stimulus duration of 1 ms. The recordings were conducted in VC mode at −55 mV holding potential, using whole-cell compensation with R_S compensation in the range of 40-60%. The series resistance was tested by a +5mV voltage step of 20 ms duration at the end of each trace. Test pulses were used to find out the minimal voltage amplitude that yielded a synaptic response in the target cell. The pipette was moved up to 3 times if no response could be elicited. We used a paired-pulse protocol (1 ms stimulus duration at 50 ms interval) to detect postsynaptic currents and the presence of short-term synaptic potentiation or depression. There was a free interval of 10 seconds to allow for regeneration of the synapses, and the protocols were repeated 10 to 40 times to average and account for the stochastic nature of synaptic transmission. To get an estimate of the receptor types involved in the synaptic transmission, the influence of the AMPA receptor blocker DNQX (10µM) and the GABA-A receptor blocker gabazine (10 µM) were evaluated. The drugs were estimated to be washed into the bath solution after 100 seconds.

4.2.2 Morphology

Single cell staining: During the recording, which lasted from 10 to 40 minutes, the cells were filled with biocytin, and afterwards fixed overnight with 4% formaldehyde in 0.1 M phosphate buffer (PB), pH 7.4 at 4°C. After fixation, the slices were rinsed extensively in 0.025 M phosphate buffered saline (PBS) and then incubated in 0.025 M PBS containing 10% normal goat serum (NGS), 0.3% Triton X-100 and 0.05% sodium azide to counter microbiological growth (1 hour, RT). After thorough rinsing in 0.1 M PB, the slices were incubated for 24 - 72 hours at 4 °C in Streptavidin-conjugated Alexa Flour 647 (Molecular Probes, 1:1000), in a solution of 3% NGS, 0.3% Triton and 0.05% sodium azide. Afterwards, the slices were washed extensively in PBS, then mounted on glass slides surrounded by a layer of agar (5% agar-agar, Roth) of 300 µm thickness and coverslipped with aqueous mounting medium (Immu-mount).
Most of the immunostainings and some of the mounting was done by Ina Wolter (MTA, Institut für Integrative Neuroanatomie, Charité - Universitätsmedizin Berlin).

4.2.3 Immunocytochemistry and *in situ* hybridization

Perfusion and preparation: Adult rats of the VGAT-Venus-A-strain were anaesthetized and killed by rapid transcardial perfusion with a fixative solution containing 4% PFA and 15% saturated picric acid in 0.1 M PBS for 30 minutes. The brains were then carefully removed from the skull, postfixed in 4% PFA for another 2-4 hours and stored overnight in 20% sucrose in 0.1 M PBS. After a short course in isopentan at−40°C, the brains were then stored at −70°C. This work was done by Samuel Booker and Anja Matthiä (both Charité - Universitätsmedizin Berlin at the time of experimentation).
Cryostat slicing: For the 50µm series of the habenula, a perfused left brain half of an adult rat was thawed in 20% sucrose solution, and the first and last fourth were removed by coronal cuts. The resulting block of tissue was then glued onto a thin layer of cork and shock-frozen in liquid hexane at −70°C. After one day in the freezer at −20°C, the liquid had evaporated, and the tissue blocks were taken to the cryostat for further processing. Coronal slices of 50 µm thickness were obtained at −25C°. For immunohistochemistry, these slices were transferred consecutively to 8 wells containing 0.1 M PB so that they could be processed together. The distance between individual slices in one direction was thus 400 µm minimum and allowed to order them correctly later.

Immunohistochemistry of 50 µm slices for neuronal markers: After thorough rinsing in 0.1 M PB (3x15 min, RT) and 0.025 M PBS (3x15 min, RT), the slices were blocked in 0.025 M PBS containing 10% normal goat serum (NGS), 0.1% Triton-X100 and 0.05% Na-Azide (1 hour, RT). The primary antibodies were then administered to the eight wells, so that every fourth section (distance approximately 200 µm) received the same primary antibody (72 hours, 4°C). The concentrations were the following - rabbit anti-parvalbumin (Swant, 1:5000), rabbit anti-calbindin (Swant, 1:2500), rabbit anti-B17 (Invitrogen, 1:800) and rabbit anti-Neu-N (Millipore, 1:1000) - and the antibodies were dissolved in a solution of 0.025 M PBS containing 5% NGS, 0.1% Triton-X100 and 0.05% Na-Azide. In addition, a mouse anti-GFP antibody (NeuroM, 1:1000) was added to each well. After washing in 0.025 M PBS (3.15 min, RT) the sections were incubated with a goat anti-mouse Alexa-488 antibody (Invitrogen, 1:500) and a goat anti-rabbit Alexa-647 antibody (Invitrogen, 1:500) for one hour at room temperature in 0.025 M PBS with 3% NGS, 0.3% Triton and 0.05% NaAzide. Afterwards, the slices were washed thoroughly in 0.025 PBS (4x15 min, RT) and 0.1 M PB (4x15 min, RT), and then mounted on glass slides and coverslipped with aqueous mounting medium.

Immunohistochemistry of 50 µm slices for GFP: 50 µm sections were washed in 0.1 M PB (3x10 min, RT) and then preincubated in 10% NGS in 0.1 M PB (30 min, RT) in order to reduce background.

Afterwards the slices were incubated with a mouse primary anti-GFP antibody (Invitrogen, 1:1000) diluted in 0.1 M PB containing 1% NGS (2-4 hours at RT, then overnight at 4°C). On the next day after thorough washing in 0.1 M PB (3x10 min, RT) the secondary antibodies were applied: goat anti-mouse Alexa Flour 488 (Invitrogen, 1:500) diluted in 0.1 M PB (3 hours, RT). The sections were then washed in 0.1 M PB (2 hours with replacement of solution several times, RT) and mounted on glass slides and coverslipped with aqueous mounting medium.

In situ hybridization for GAD67: For the *in situ* hybridization, 50 µm cryostat sections were preincubated in hybridization buffer (HB) diluted with 2x saline sodium citrate (SSC, 1:1) for 15 minutes, and then prehybridized in HB for 60 minutes at 45°C. Using the same buffer and DIG-labeled GAD67 anti-sense or sense cRNA probes (50 ng/ml), the sections were hybridized overnight at 45 °C. After the hybridization, the sections were rinsed in 2x SSC (2x15 min, RT), 2x SSC and 50% formamide (15 min, 55°C), 0.1x SSC (2x15 min, 55°C), and finally in Tris-buffered saline (1% blocking solution in TBS, 60 min, RT). The DIG-labeled hybrids were then incubated with an anti-DIG antibody conjugated with

alkaline phosphatase (1:1500, sheep, Roche) in 1% blocking solution and left overnight at 4°C. On the following day, the sections were washed in TBS pH 7.5 (2x10 min, RT) and substrate buffer (1x10 min, RT). Next, the substrate solution was added, and the sections were monitored for adequate staining intensity. Finally, the sections were coverslipped in Kaiser's glycerol gelatin. The slices were imaged using bright field microscopy (Axiovision 4.8 Zeiss), and the correct labeling was confirmed in the hippocampus, an area with a well-described distribution of GABAergic neurons.

The immunohistochemistry for GFP and the *in situ* hybridization for GAD 67 were performed by Susanne Huber (Labor für Experimentelle Epilepsieforschung, Universität Freiburg). The evaluation under the microscope, as well as major parts of the analysis of the images, was done by Anja Matthiä (former Charité - Universitätsmedizin Berlin).

Confocal microscopy of 300 µm slices: Using a fluorescence confocal microscope (FV1000 Olympus with x20 objective, numeric aperture 0.75) and a 635 nm laser, image stacks of the patched and visualized neurons were acquired. The images were taken at a distance in the z-direction of 1 to 1.25 µm, and both laser intensity and the threshold were adjusted to ensure an even brightness throughout the image stack.

Colocalization analysis: The cell body of the neuron was imaged separately using a 488 nm laser to confirm the YFP labeling of the cell indicative of Venus-expression. The 635 nm laser was used to evaluate for colocalization with the biocytin labeling.

Reconstruction and analysis: From the image stacks, cells were reconstructed semi automatically using the Simple Neurite Tracer plugin in ImageJ. After tracing the dendrites and axon of the neuron emerging from the soma, the neuron could be virtually "filled" to distinguish between true signal and background.

Measurements: Using a z-projection of the entire stack, extension of the neuron in both medio-lateral (*width*) and superior-inferior (*height*) direction were measured using ImageJ. The same was done for the cell body of the imaged neuron. If a primary dendrite was cut, the neuron was excluded from morphological analysis.

Neuronal marker series: The slices were imaged as stacks of 2 µm slice thickness at x20 magnification. The YFP+ neurons located in the LHb were then evaluated for colocalization with the respective neuronal marker by creating an overlay of the images from the 488 nm and the 635 nm laser.

4.2.4 Data analysis

Data were analyzed using Stimfit 0.10 and the inbuilt Python environment.

V_{REST}, R_{in}, τ: The resting membrane potential was determined in I=0 mode in the first minute after breakthrough. Any cells being more depolarized than −45 mV were discarded from further analysis. For the input resistance and membrane time constant, traces that contained action potentials or marked post synaptic potential were discarded, and the remaining were averaged. R_{in} was calculated using Ohm's law by dividing the resulting drop in membrane potential by the amount of injected current in steady state. τ was determined by fitting both a mono- as well as a biexponential curve to the decay of membrane potential after brief −1 nA stimulation back to baseline. If the biexponential fit was more accurate, and showed a lower sum of squared errors (SSE), the longer time constant was taken as τ.

R_S and C_M: The series resistance R_S was calculated using Ohm's law by measuring in VC the initial fast component of the response to a −5 mV hyperpolarizing pulse. C_M was calculated using the following equation: $C_M = [\tau_1 \frac{1}{R_S}(\frac{I_1}{I_1+I_2}) + \tau_2 \frac{1}{R_S}(\frac{I_2}{I_1+I_2})] \frac{R_S+R_M}{R_M}$, with τ_1 being the fast and τ_2 being the slow time constant, and I_1 and I_2 the respective amplitudes of a biexponential fit of the decay curve from the negative peak to steady state (Booker et al. 2013). R_M was calculated from the difference between current flow in steady state and at baseline divided by −5 mV.

f_{200pA}, f_{INST}, accommodation-index: In the traces with +200 pA current input from a holding potential of −65 mV in CC, the firing frequency was calculated with a built-in function in Stimfit. The interspike intervals (ISIs) were measured as the time between two neighboring APs. The instantaneous firing frequency was calculated as the reciprocal of the first ISI, and the accommodation-index calculated as the ratio of ISI_{LAST} and ISI_{MIDDLE}.

AHP, Sag-index: The afterhyperpolarization in the 200 pA traces was defined as the peak negative potential measured from baseline after the train of APs, before the neuron returned to holding potential. The Sag index was analyzed in the −50 pA stimulation trace and was calculated as the relative extent of the negative deflection of the membrane potential in the first 100 ms of current injection compared to steady state.

Action potential analysis: In the recordings at −55 mV holding potential, the trace was selected in which the smallest depolarizing current pulse elicited at least two subsequent APs. The current pulse amplitudes (rheobase) ranged from 10 to 50 pA for these traces. All measurements were taken from *threshold,* defined as the voltage value of the sampling point at which the differential of the voltage first exceeded 20 mV/ms.

(1) The *amplitude* was measured from threshold in mV.

(2) The magnitude of the *fast afterhyperpolarizing potential (AHP_{fast})* was measured from threshold as the maximal negative inflection immediately following the peak of the AP.
In the −55 mV trace, in which the cells responded with single AP firing instead of bursts, an *afterdepolarizing potential (ADP)* was also usually present, forming a small "hump" in the trace. These were followed by a further slower negative deflection, termed *medium afterhyperpolarizing potentials (AHP_{medium}).* If these potentials were present, the amplitude of the *ADP* was measured from the most negative point of the AHP_{fast}, and the amplitude of the AHP_{medium} from threshold.
Excitatory and inhibitory postsynaptic currents (EPSCs and IPSCs): The recorded traces were averaged, and the *amplitudes* of the PSCs were measured as the peak following the stimulus artifact relative to preceding baseline. To estimate the *decay time constant* of the synaptic responses, a monoexponential curve was fitted by the method of the least sum of squared errors. *Synaptic transmission rate* was determined by scanning the traces for PSCs that exceeded the baseline noise by a factor of 5 (i.e. 5 times larger than the standard deviation of the baseline). The *paired-pulse ratio (PPR)* was defined as the amplitude ratio of the second and the first PSC.

All data are reported as mean ± SD. To evaluate statistical significance, the Mann-Whitney-U-Test was used for comparison between the populations of YFP+ and YFP− cells, and the Kruskal-Wallis-Test for comparison of different groups of the YFP+ cells.

5 Results

5.1 Distribution of YFP+ and GAD67+ neurons in the LHb

Interneurons in the cortex and thalamus have a predominant inhibitory effect postsynaptically and use GABA as their primary neurotransmitter (Arcelli et al. 1997; Soltesz 2006). They express glutamate acid decarboxylase (GAD), the enzyme that synthesizes this neurotransmitter and a vesicular GABA transporter (VGAT). GAD has two isoforms, one of 67 kD weight (GAD67), which is ubiquitously present in GABAergic cells, and another with 65 kD weight (GAD65) preferentially localized to axon terminals, as does VGAT. In the present experiments, we have used a transgenic line, VGAT-Venus-A rats, in which the yellow fluorescent protein (YFP) Venus is expressed under the promoter of the vesicular GABA transporter (VGAT). The promoter ensures the correct expression of the transgene, however, there is evidence that mis-expression of fluorescent markers may occur in some brain areas in such transgenic lines (Meyer et al. 2002). To evaluate whether YFP+ neurons in the LHb are GABAergic we compared 50 µm brain sections of an adult VGAT-Venus-A animal alternately stained with *in situ* hybridization against GAD67-RNA and with immunohistochemistry using an anti-GFP antibody that intensified the YFP signal.

When comparing the *in situ* hybridization with the anti-GFP immunohistochemistry we found two distinct populations of neurons. GAD67-expressing neurons cluster in the caudal half of the habenula in the lateral aspect of the LHb (Fig. 6 right panel). The medial part of the LHb was virtually void of GAD67-expressing cells. The VGAT-Venus-positive neurons on the other hand were preferentially located near the border of the MHb and the LHb, although some were scattered throughout the LHb and also intercalated in the *stria medullaris (*Fig. 6 left panel). Remarkably a cluster of YFP+ cells was found in the caudal slices located ventrally, close to the paraventricular nucleus of the thalamus (Fig. 6 left panel). This cell group was also regularly encountered in *in vitro* slices during experiments (Fig. 7).

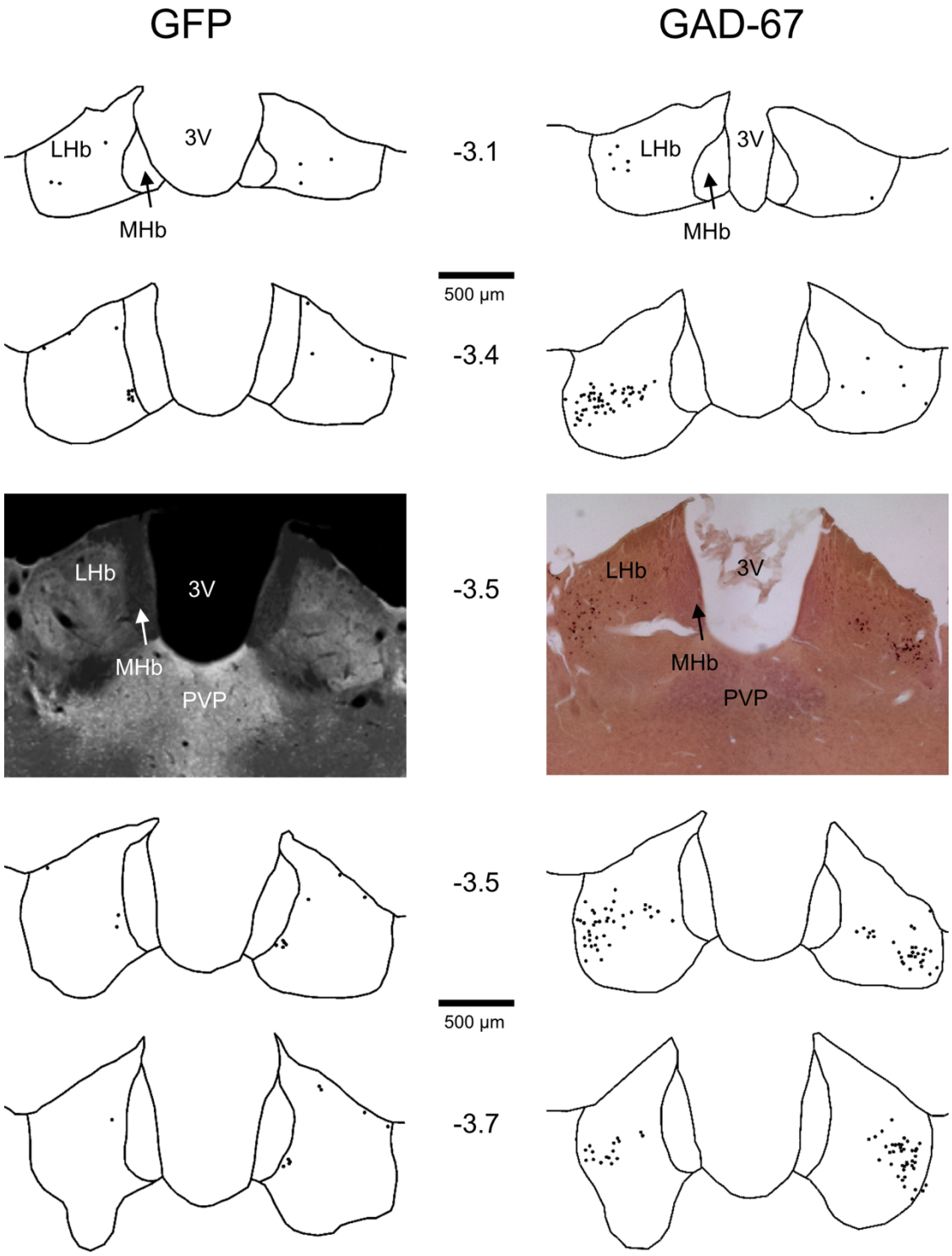

Figure 6: GAD67 expressing GABAergic neurons and GFP/YFP+ neurons form distinct populations in the habenula.

Representative sections of the habenula at different cranio-caudal distances from Bregma (levels indicated by the numbers expressed in mm). Black dots in the camera lucida drawings indicate the localization of the labeled cells. Note the virtual absence of GFP/YFP+ neurons in the medial habenula (MHb) and in the lateral part of the lateral habenula (LHb, left panel), and the clustering of GAD-67-positive cells in the lateral and caudal aspect of the LHb (right panel).

Abbreviations: 3V - third ventricle, PVP - posterior paraventricular thalamic nucleus.

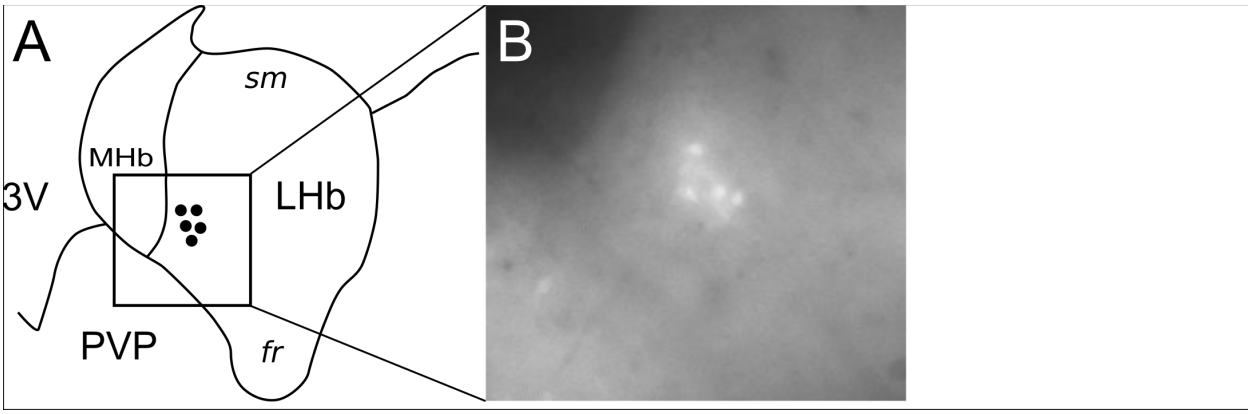

Figure 7: A subset of YFP+ cells localized to the caudal habenula observed in an acute slice.

A: Diagram depicting the position of the neurons inside the habenula **B:** Visualization by epifluorescence during whole-cell patch clamp experiment. The YFP+ cell cluster was localized to the lateral habenula (LHb) directly at the border to the medial habenula (MHb) and ventrally, in close proximity to the posterior paraventricular nucleus of the thalamus (PVP).

Abbreviations: 3V - third ventricle; *fr – fasciculus retroflexus; sm – stria medullaris.*

5.2 Neuronal markers in YFP+ cells

To further characterize the population of YFP+ cells in the LHb, we evaluated the presence of three neuronal markers in these cells. Parvalbumin (PV) and calbindin (CB) are calcium-binding proteins that are expressed by subsets of interneurons in other parts of the central nervous system (Tremblay, Lee, and Rudy 2016). GABA-B receptor on the other hand was reported to be strongly expressed by neurons in the medial part of the LHb (Geisler, Andres, and Veh 2003), i.e. the primary location of YFP+ cells. Therefore, we performed immunohistochemistry for these markers in a series of slices of the habenula of an adult VGAT-Venus-A rat. In this series, subsequent slices were stained for either of the three markers - PV, CB, and GABA-B receptor - in an alternating manner. PV-positive cells in the LHb were sparse (n=15), and none of them showed co-labeling for YFP (Fig. 8A). Calbindin was found to be strongly expressed in a region bordering the MHb, but weaker labeled cells were found throughout the LHb (Fig. 8B). Only 10 out of 177 cells analyzed showed double-labeling with CB and YFP, and 8 of these formed a group of cells intercalated in the *stria medullaris* (Fig. 8C), suggesting that they may constitute a specific type. The content of GABA-B receptor appeared to be sparse in the LHb compared to the MHb. The labeling was preferentially found on the cell bodies in contrast to the intensive labeling of fibers in the MHb. However, none of the cells labeled for GABA-B receptor was co-labeled for YFP.

In summary, YFP+ neurons in the lateral habenula do not express the typical interneuronal markers PV or calbindin, or the metabotropic GABA-B receptor, which otherwise is highly expressed by habenular neurons.

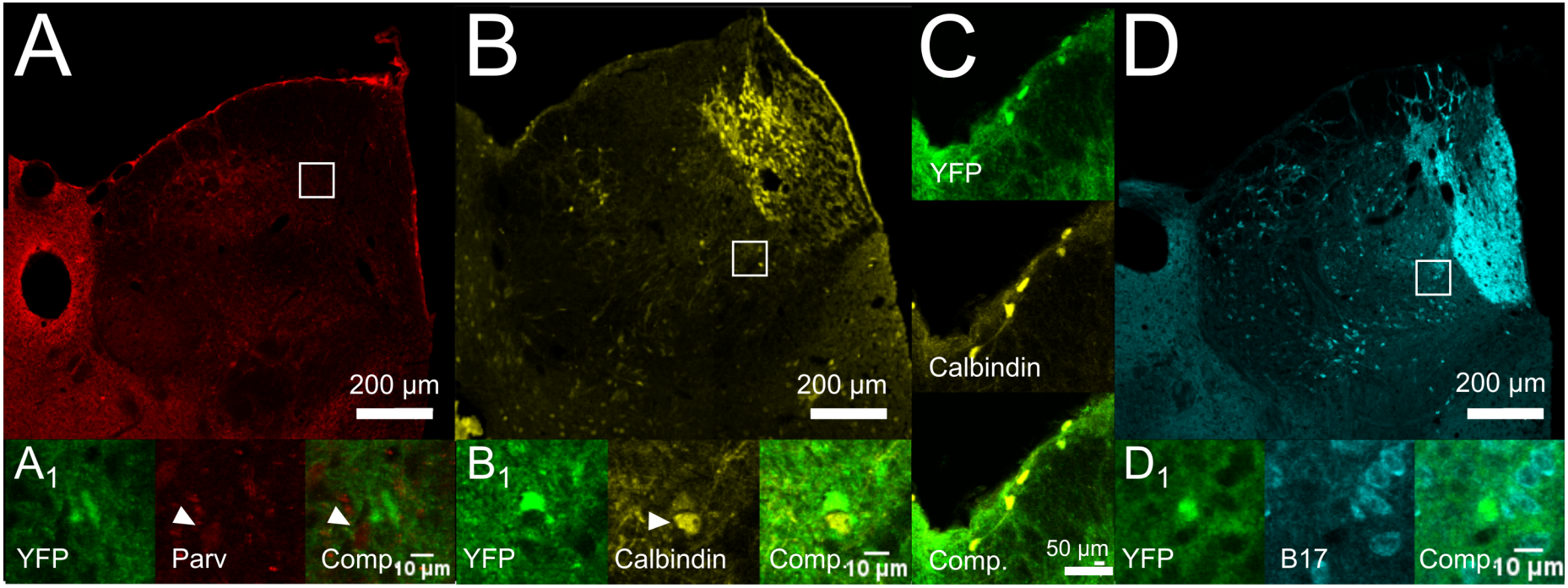

Figure 8: Labeling for neuronal markers Parvalbumin, Calbindin and GABA-B receptor in comparison to YFP+ neurons in the habenula.

A: Immunofluorescence labeling shows that Parvalbumin (in red pseudocolour) is only weakly expressed in the LHb. **A1** High magnification images illustrate two YFP+ cells that are not labeled for PV, and one additional weakly PV-labeled cell (arrowhead). **B:** Calbindin+ neurons (yellow) are present throughout the LHb. Note the weak calbindin labeling in a YFP+ cell in **B1** (arrowhead). **C** shows a small population of YFP+ cells in the *stria medullaris* strongly co-labeled for calbindin. **D and D1:** Several neurons in the LHb express GABA-B receptor in their somata, but were not YFP+.

5.3 Morphological properties of LHb neurons

Different classes of neurons show distinct cell morphologies. Importantly, the distribution of the dendrites defines the input region of a neuron, whereas the axon projects towards the output region. With respect to the axon, two different cell classes can be defined: (1) projection neurons show an axon projecting to other brain areas, whereas (2) local circuit interneurons have a dense local axon, collateralizing in the same region.

In whole-cell patch clamp experiments neuron morphology was acquired by filling the cells with biocytin during the recordings. After the experiments, neurons can be visualized with streptavidin coupled to a fluorescent dye, e.g., Alexa-647. Neurons were obtained mostly in the medial part of the LHb due to their higher density in this area (compare Fig. 6 left panel). For quantitative analysis of cell dimensions and morphological properties only neurons with intact primary dendrites were considered. The mediolateral and dorsoventral extension of the dendritic tree was measured as the sides of the bounding rectangle.

The typical appearance of a YFP+ neuron was as follows: From the soma 3-4 dendrites extended in a vertical fashion. These dendrites branched sparsely and showed regular swellings. The axon arose from the soma or a primary dendrite and branched only in a small number of cells. Its course was heterogenous and small varicosities, suggestive of boutons-en-passant, were noted along its course. An example of a YFP+ neuron including its basic electrophysiological behavior and firing pattern is given in Figure 9.

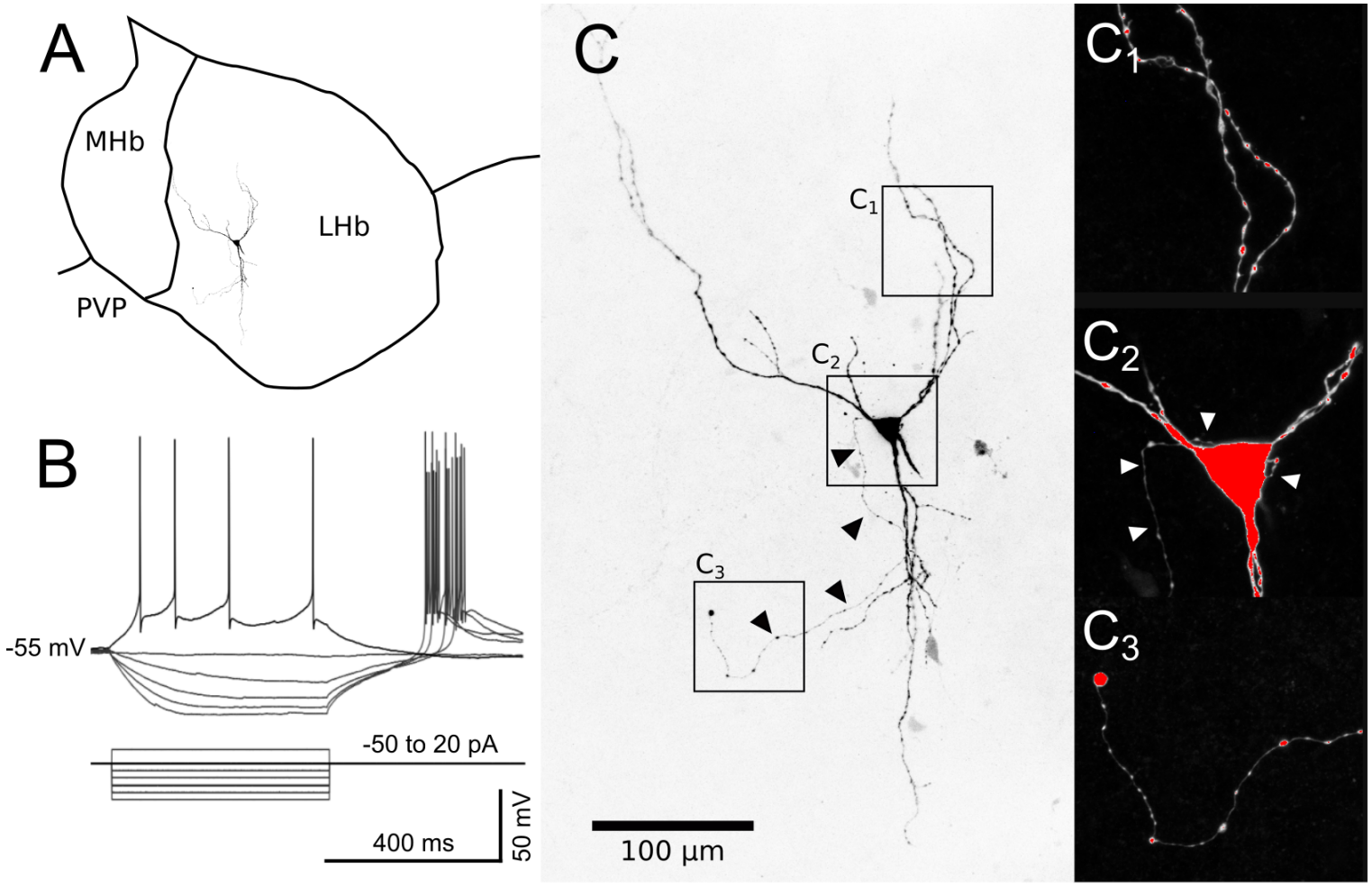

Figure 9: Morphology and physiological properties of a YFP+ neuron.

A: Diagram illustrating the position of the neuron inside the habenula. **B:** Voltage responses of the neuron to hyperpolarizing and suprathreshold depolarizing current pulses. Note the rebound bursting after the hyperpolarization. **C:** A projection of the confocal image stack depicting the neuron. Arrowheads indicate the axon.**C_1:** Higher magnification images of two dendrites (upper box in C) illustrate the dendritic beads and lack of spines. **C_2:** High magnification image of the axon arising from the soma (middle box in C). White arrowheads mark the path of the axon. **C_3:** High magnification image of the axon illustrates swellings along its path. The axon is cut at the surface of the slice.

5.4 Groups of YFP+ neurons

Based on their localization and morphological appearance, YFP+ cells were assigned to three different groups:

5.4.1 Ventral YFP+ cells with a dendritic tuft in the PVP

A group of YFP+ cells (n=24) with a dendritic tuft in the posterior paraventricular nucleus of the thalamus (PVP) was found in close proximity to the border of the MHb, in the ventral part of the LHb. Frequently, a small group of 5-10 densely packed YFP+ cells could be observed here (Fig. 7).

Their cell bodies varied from round to oval and measured 14.8 ± 2.2 by 10.8 ± 1.8 µm in size. The somata gave rise to 3 or 4 primary dendrites which did not branch extensively and had no spines (Fig. 10). All of these cells were orientated vertically – i.e., their primary dendrites extended in a ventro-dorsal fashion – and covered an area of 407.5 ± 78 times 412.1 ± 107.9 µm. Although located close to the border of the MHb, the dendrites did not cross it. In contrast, a striking feature of these neurons was their extensive dendritic tuft extending into the posterior paraventricular thalamic nucleus (PVP). One or two of their primary dendrites extended ventrally, with minimal or no branching prior to the *fasciculus retroflexus*. In the PVP these dendrites started to branch forming a small tuft, but the dendritic processes did not cross the midline (Fig. 10).

YFP− cells patched in the same region did not extend their dendrites in the PVP, nor in other regions of the thalamus. In other research, a small number of glutamatergic LHb neurons have been reported to extend single dendrites into the thalamus (Weiss and Veh 2011).

The axon could be identified unequivocally in 20 of the 24 YFP+ cells with a dendritic tuft in the PVP. In 9 cells, however, the axon was cut on the surface of the slice shortly after emerging from the cell. In the remaining 11 cells, the axon could be followed over a longer distance. Although the axons of these cells showed substantial differences in their trajectory, they showed no substantial branching or local collateralization. This thick non-branching axon was consistent with a population of projection neurons, rather than local circuit interneurons.

Interestingly, in 6 neurons of this group the axon turned rostrally. Due to the scarcity of YFP+ neurons in the LHb, we failed to examine the projection target of these cells in sagittal slices.

5.4.2 YFP+ cells without a dendritic tuft in the PVP

An additional YFP+ group of neurons were found slightly more dorsally in the medial part of the LHb. Like the neurons with a dendritic tuft in the PVP, these neurons (n=12) displayed small somata (15.2 ± 2.2 by 11.4 ± 1.8 µm) giving rise to 3 to 5 primary dendrites that branched sparsely and had no spines. The dendritic arbor was vertically orientated and covered a smaller area (262.8± 104.2 µm in the mediolateral and 334.7 ± 112.4 µm in the dorsoventral direction) without crossing the boundaries of the habenula. In some cells a single dendrite extended into the *stria medullaris* (Fig. 11, neurons 6 and 7). The YFP+ cells without PVP-dendrite could not be distinguished from YFP− cells on the basis of morphological parameters alone.

The axon was identified in 10 out of 12 cells but was cut near the surface in 5 of them. In 5 cells it could be followed deep into the slice, and it joined the *fasciculus retroflexus* in 4 of the cells, again indicating that these cells comprise a subset of projection neurons. In the remaining one the axon ran caudo-laterally to the thalamus.

5.4.3 YFP+ cells located in the *stria medullaris*

A further group of YFP+ neurons were found dorsally in the LHb in or near the *stria medullaris*. Due to the large amount of fibers only cells lying superficially intercalated in the *stria medullaris* could be patched, therefore only four cells (n=4) were retrieved with their dendritic arbor intact. These strial cells had small cell bodies which measured on average 14.4 ± 2.1 µm in length and 10.6 ± 2.4 µm in width. 2 or 3 primary dendrites arose from the somata in all directions, and did not extend much within the *stria medullaris*, but turned ventrally in the medial part of the LHb (Fig. 12). The dendritic area covered 288.2 ± 88.4 µm by 179.3 ± 35.0 µm on average. Similar to the other two groups, no spines were observed on the dendrites.

In 2 of the 4 neurons the axon could be followed deep into the slice and ran latero-caudally towards the *fasciculus retroflexus*, an indication that these cells are likely to be projection neurons, as well.

5.4.4 YFP− cells

Similar to the second group of YFP+ cells, YFP− cells displayed small somata and a bipolar to triangular appearance of the dendritic tree where the basal and the apical dendrites were of similar appearance and magnitude (Fig. 13). In 9 cells retrieved with

their primary dendrites intact, cell bodies measured on average 17.9 ± 3.8 µm in length and 13 ± 1.9 µm in width. Their dendrites span an area of 270.5 ± 60.1 µm in mediolateral and 331.5 ± 14 µm in dorsoventral direction. The dendritic branches were aspiny. These observations were consistent with previous work on the morphology of these cells (Kim and Chang 2005; Weiss and Veh 2011). Their axons all traveled caudally and ventrally to join the *fasciculus retroflexus*, the main output of the habenula, and no branching was observed in any of them.

In summary, the four groups of neurons showed strong similarities. Their dendrites extend typically in the vertical direction and although they cover relatively large areas, they branch sparsely. No spines could be found on the dendrites.

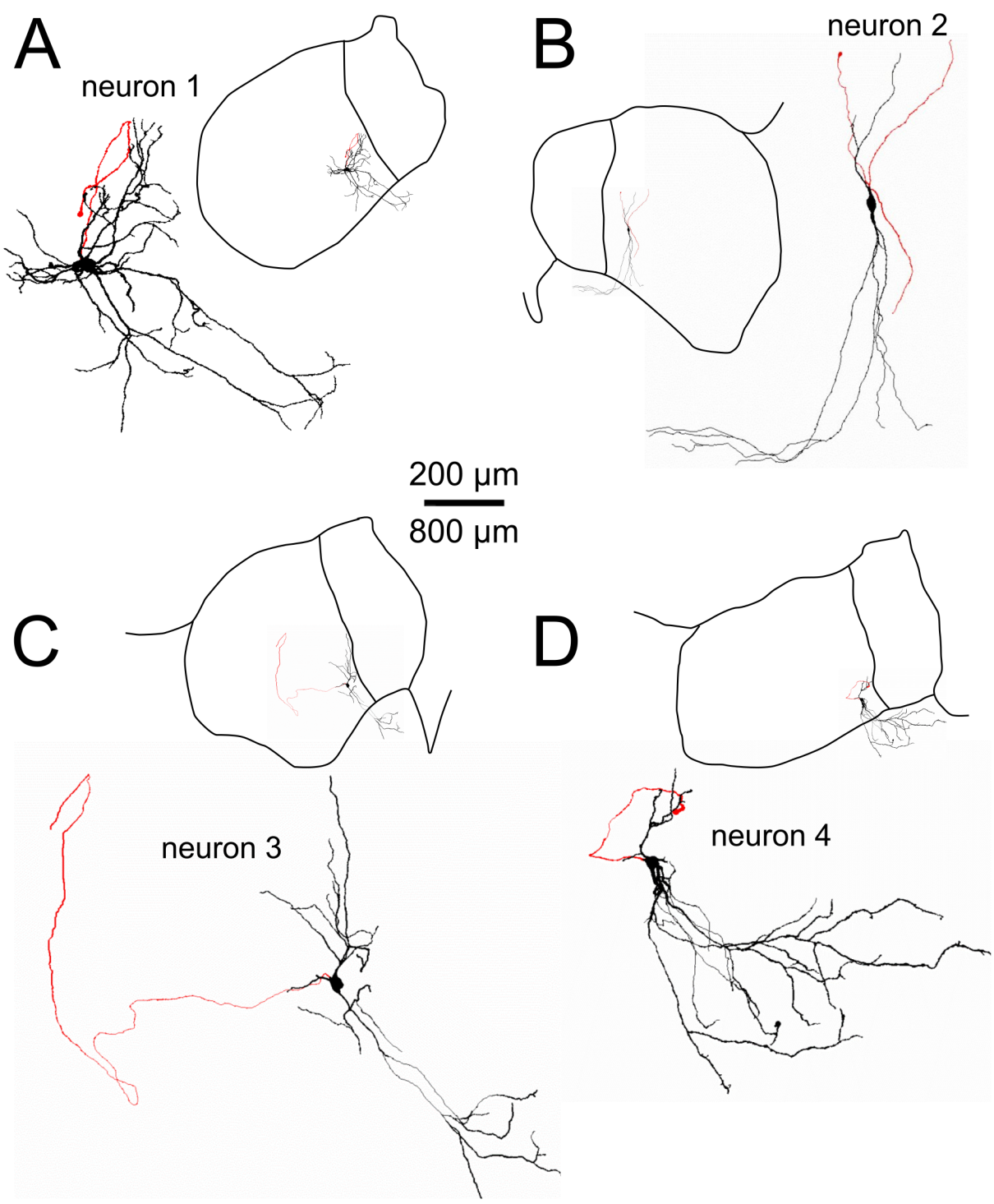

Figure 10: Morphology of ventral YFP+ neurons with a dendritic tuft in the posterior paraventricular thalamic nucleus (PVP).

Full reconstructions of recorded and biocytin-filled YFP+ neurons from confocal image stacks. The axons are displayed in red and a smaller reconstruction of each cell is superimposed on the outlines of the habenula to illustrate the location in the LHb. The scale bar represents 200 µm for the reconstructions and 800 µm for the habenula outlines.

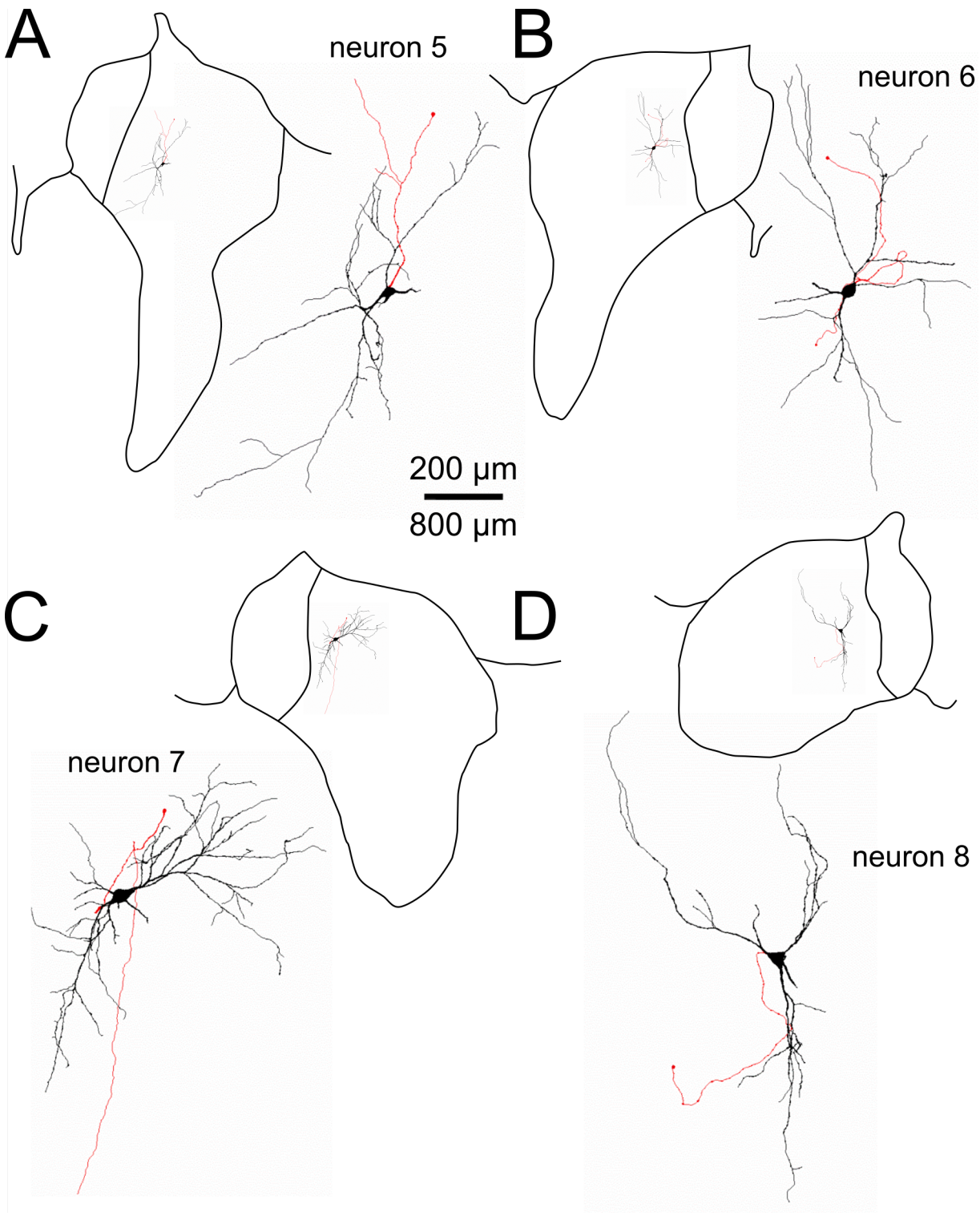

Figure 11: Morphology of YFP+ neurons without a dendritic tuft in the posterior paraventricular thalamic nucleus (PVP).

Full reconstructions of recorded and biocytin-filled YFP+ neurons from confocal image stacks. The axons are displayed in red and a smaller reconstruction of each cell is superimposed on the outlines of the habenula to illustrate the location in the LHb. The scale bar represents 200 µm for the reconstructions and 800 µm for the habenula outlines.

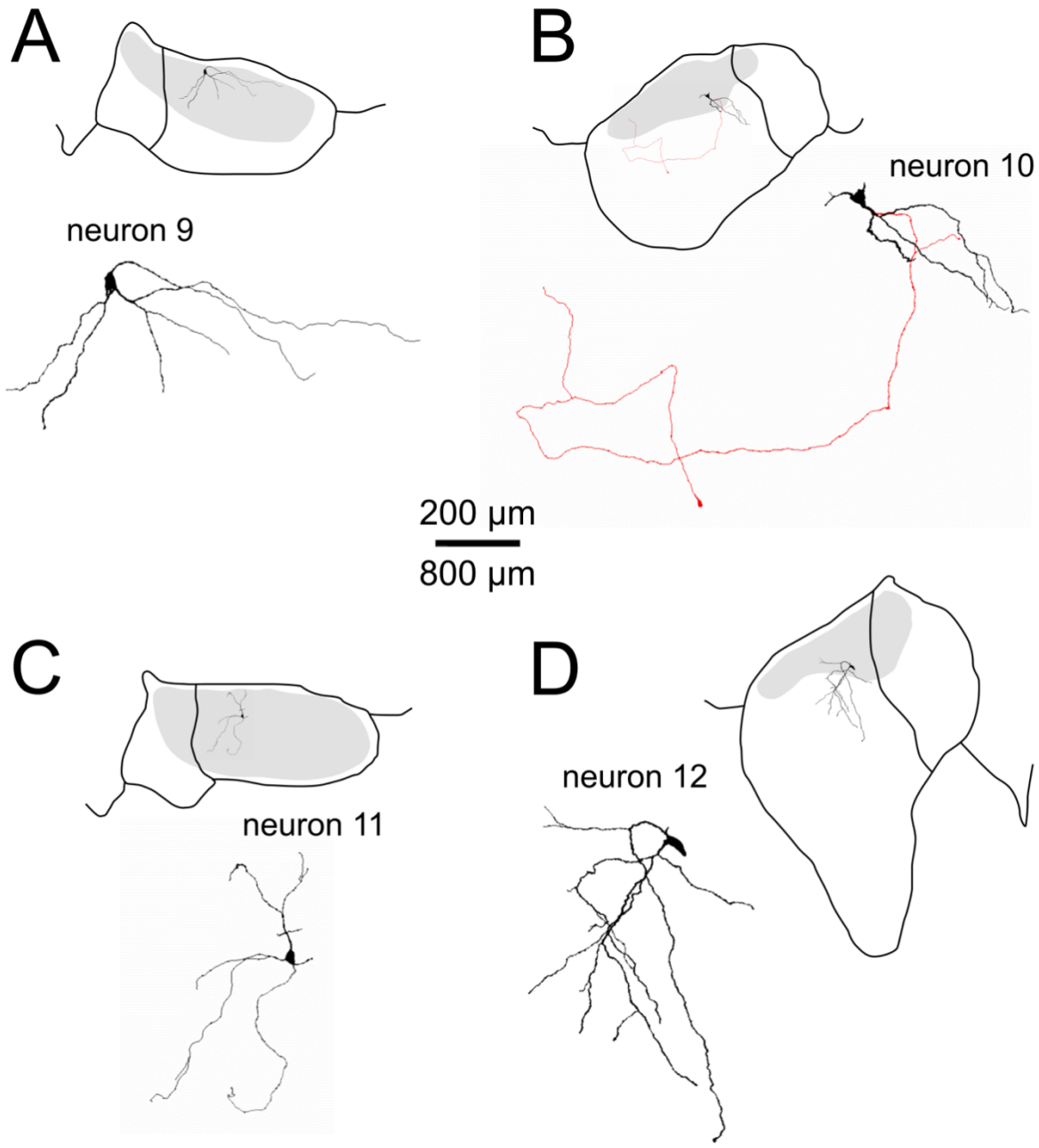

Figure 12: Morphology of YFP+ neurons located in the *stria medullaris.*

Full reconstructions of recorded and biocytin-filled YFP+ neurons from confocal image stacks. The axons are displayed in red and a smaller reconstruction of each cell is superimposed on the outlines of the habenula to illustrate the location in the LHb. The scale bar represents 200 µm for the reconstructions and 800 µm for the habenula outlines. The outlines of the *stria medullaris* are marked in grey.

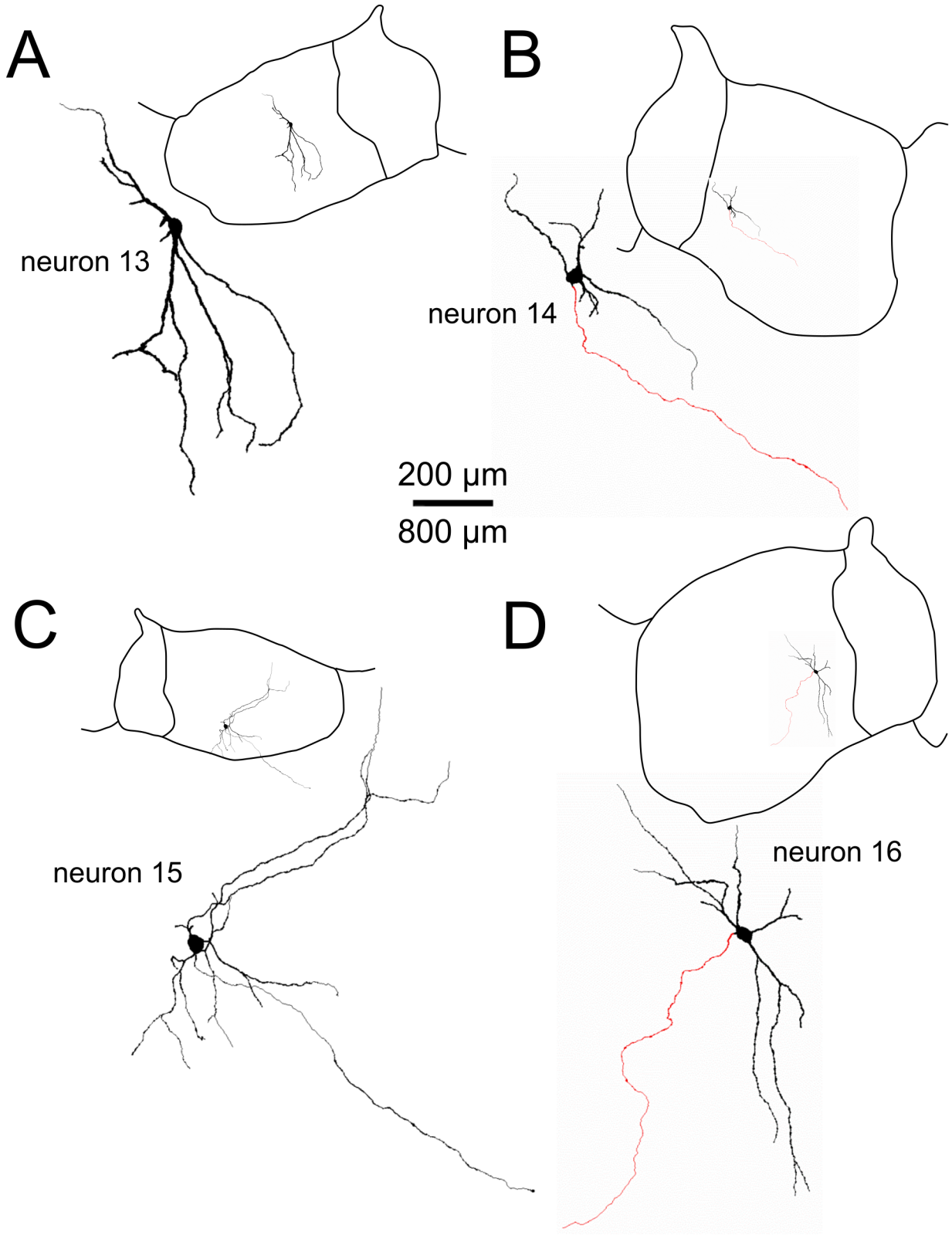

Figure 13: Morphology of YFP– neurons in the lateral habenula.

Full reconstructions of recorded and biocytin-filled YFP+ neurons from confocal image stacks. The axons are displayed in red and a smaller reconstruction of each cell is superimposed on the outlines of the habenula to illustrate the location in the LHb. The scale bar represents 200 µm for the reconstructions and 800 µm for the habenula outlines.

5.5 Electrophysiological properties of YFP+ and YFP− cells in the LHb

The electrophysiological properties are essential determinants of the function of a neuron, and different neuronal classes usually differ in their firing patterns and their response to stimulation. To assess the electrophysiological properties of YFP+ and YFP− cells in the LHb, whole-cell patch clamp experiments were performed on both cell types.

Using fluorescence video microscopy, cells could be determined as either YFP+ or YFP− and then targeted for recording (Fig. 5, see also the Methods). After breaking into the cell, the resting membrane potential was recorded and different protocols (see Methods) were run to assess passive membrane properties such as input resistance (R_{IN}), membrane time constant (τ) and membrane capacitance (C_M). To evaluate subthreshold and active firing properties, cells were hyper- as well as depolarized by current pulses of −100 pA to +200 pA amplitude.

A total of 57 YFP+ and 24 YFP− cells were included in the analysis. The results of all analyzed measurements are summarized in Tables 7 and 8.

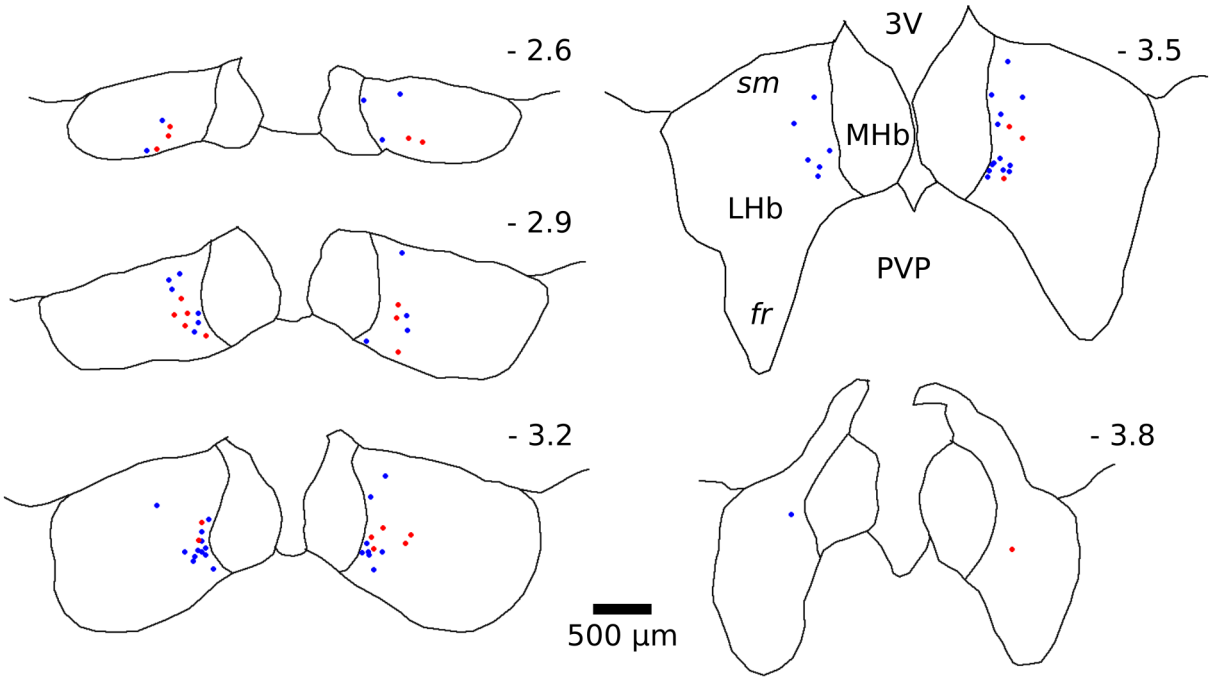

Figure 14: Position of the recorded neurons, used in this study, within the habenula.

Numbers beside the panels indicate the distance from bregma in mm. YFP+ cells are represented by blue dots, YFP–cells by red ones. Note that the recorded neurons are confined to the medial part of the lateral habenula (LHb) because the number of YFP– cells was far higher compared to the lateral one.

Abbreviations: 3V - third ventricle; *fr* - *fasciculus retroflexus;* LHb - lateral habenula; MHb - medial habenula; PVP - posterior nucleus of paraventricular thalamus; *sm* - *stria medullaris.*

The location of the recorded neurons within the habenula is shown in Figure 15 and displays a strong bias towards the medial part of the LHb. This is mainly due to the scarceness of YFP+ cells in the lateral part of the LHb – i.e., it reflects the distribution of YFP+ neurons within the habenula well (compare Figure 6 left panel). A large portion of the patched YFP+ cells are located in the caudal LHb near both the border to the MHb and the PVP. These neurons usually extended their basal dendrite into the PVP (Fig. 10).

On average YFP+ cells were found to be slightly more hyperpolarized in resting membrane potential (V_M) (YFP+: –61.0 mV ± 8.7 vs. YFP–: –57.0 mV ± 6.4; n.s). Both cell populations were found to be electrically compact with an input resistance of around 900 MΩ, although high variability was observed, reflected by the large standard deviation (YFP+: 889.2 MΩ ± 416.2 vs. YFP–: 884.9 MΩ ± 358.8; n.s.). The comparison of the cell capacitance (C_M) suggests that YFP+ cells are significantly larger than their YFP–counterparts (YFP+: 68.9 pF ± 34.1 vs. YFP–: 48.1 pF ± 24.7 $p<0.01$).

The response to hyperpolarizing current pulses was different between the two groups. Although the membrane time constant (τ) was similar (YFP+: 61.9 ms ± 23.6 vs. YFP– 61.3 ms ± 21.6; n.s.), the YFP– neurons showed a higher degree of delayed inward rectification as illustrated by a higher Sag index (YFP+: 3.3 % ± 4.3 vs. YFP–: 7.3 % ± 6.8; $p<0.01$).

Similar to other neurons in the diencephalon, habenular neurons showed a prominent burst response following depolarization from a membrane potential more negative than –60 mV (Fig. 15A/B and 16 A/B). This was observed in all cells regardless of their YFP expression, but this burst only triggered a sustained firing in the YFP– cells (Fig. 16 A). In addition, the burst response in YFP– neurons was found to be more prominent, always yielding 3 or more action potentials and showing a higher instantaneous firing rate (YFP+: 203.6 Hz ± 69.1 vs. YFP–: 263.2 ± 121.4; n.s.). The firing rate in response to a depolarizing current pulse of 200 pA ($f_{200\ pA}$) was similar between the two groups (YFP+: 65.0 Hz ± 16.5 vs. YFP– 71.1 Hz ± 30.3; n.s.). Here YFP– neurons displayed a higher degree of accommodation (accommodation index: YFP+: 12.1 % ± 12.6 vs. YFP–: 42.2 % ± 32.3; $p<0.01$). Following a train of action potentials, both groups of neurons showed a negative deflection in membrane potential, termed *slow afterhyperpolarization (*AHP_{slow}*,* Fig. 16 D*)* (YFP+: –0.7 mV ± 2.9 vs. YFP–: –2.1 ± 4.0; n.s.).

Following depolarization from a membrane potential of –55 mV, single action potentials and trains of action potential could be elicited without bursting. The analysis of single action potentials revealed further differences between YFP+ and YFP–cells. The mean AP amplitude was larger in YFP+ cells (YFP+: 69.6 mV ± 8.4 vs. YFP–: 51.8 mV ± 11.8; $p<0.01$), and although a similar proportion of neurons in both groups showed an *afterdepolarizing potential (ADP, Fig. 15 E)* (YFP+: 63.6 % vs. YFP–: 61.9 %)*,* this was far more pronounced in YFP+ cells (YFP+: 3.7 mV ± 2.6 vs. YFP–: 0.8 mV ± 0.7). Other parameters of single action potentials, such as the threshold and the duration of the action potential and the degree of fast and medium afterhyperpolarization, (*AHP_{fast} and AHP_{medium}*) were similar between the two groups (Table 7).

Taken together, YFP+ and YFP– cells displayed similarities, but could be distinguished clearly based on their electrophysiological parameters. Figures 15 and 16 show recorded traces of a typical YFP+ and a YFP–neuron, respectively.

Comparing the three subgroups of YFP+ neurons, only minor differences were found. The cells located in the *stria medullaris* were more depolarized in their resting membrane potential (PVP-dendrite: −61.5 mV ± 8.9 vs. No PVP-dendrite: −64.3 mV ± 7.7 vs. Stria cell: −53.8 mV ± 5.5; $p<0.01$) and their total cell capacitance was smaller (PVP-dendrite: 80.4 pF ± 37.6 vs. No PVP-dendrite: 66.2 pF ± 23.1 vs. Stria cell: 39.2 pF ± 18.7; $p<0.01$). This is in good agreement with their morphological appearance as small cells without an extensive dendritic tree. The two other groups of YFP+ cells, namely those with and without a dendritic tuft in the PVP, instead appeared as a homogeneous group with comparable electrophysiological properties. The only notable difference was a smaller AHP_{slow} in YFP+ cells with a dendrite in the PVP compared to the other two subgroups (PVP-dendrite: 0.6 mV ± 2.5 vs. no PVP-dendrite: −1.9 mV ± 1.6 vs. stria cell: −3.1 ± 3.8; $p<0.01$). Additionally, the characteristics of the action potential were very similar between the three groups of YFP+ neurons (Table 8).

	YFP+	YFP–	p value
V_M (mV)	–61.0 ± 8.7	–57.0 ± 6.4	n.s.
R_{IN} (MΩ)	889.2 ± 416.2	884.9 ± 358.8	n.s.
τ (ms)	61.90 ± 23.62	61.28 ± 21.58	n.s.
C_M (pF)	68.92 ± 34.07	48.09 ± 24.67	<0.01
Sag index (%)	3.3 ± 4.3	7.3 ± 6.8	<0.01
AHP_{slow} (mV)	–0.7 ± 2.9	–2.1 ± 4.0	n.s.
f_{inst} (Hz)	203.6 ± 69.1	263.2 ± 121.4	n.s.
$f_{200\ pA}$ (Hz)	65.0 ± 16.5	71.1 ± 30.3	n.s.
accommodation index (%)	12.1 ± 12.6	42.2 ± 32.3	<0.01
number of cells (n)	57 (56 in τ, 52 in C_M)	24 (22 in τ, 23 in C_M)	

	YFP+	YFP–	p value
AP amplitude (mV)	69.6 ± 8.4	51.8 ± 11.8	<0.01
AP threshold (mV)	–28.0 ± 4.2	–29.0 ± 4.5	n.s.
AP duration (ms)	0.70 ± 0.15	0.76 ± 0.20	n.s.
AHP_{fast} (mV)	–20.4 ± 4.9	–18.9 ± 5.5	n.s.
AHP_{medium} (mV)	–18.8 ± 3.9	–22.0 ± 5.6	<0.05
ADP (mV)	3.7 ± 2.6	0.8 ± 0.7	<0.01
ADP present (%)	63.6	61.9	n.a.
number of cells	55 (53 in AHP_{fast})	21	

Table 7: Summary of active and passive membrane properties and firing properties of YFP+ and YFP– neurons in the LHb.

Abbreviations: VM - resting membrane potential; R_{IN} - membrane input resistance; τ - membrane time constant; C_M - cell capacitance; Sag index - degree of slow inward rectification; AHP - afterhyperpolarization following a train of action potentials; f_{INST} - estimated instantaneous firing frequency; $f_{200\ pA}$ - average firing rate in 200 pA stimulation from –65 mV; accommodation index - comparison of the interspike intervals from the middle and the end of a train of action potentials elicited by 500 ms of 200 pA stimulation; AP - action potential; AP threshold - membrane potential where the slope of the AP equals 20 mV/ms; AHPfast - fast afterhyperpolarizing potential hyperpolarization immediately following the peak of the AP measured from threshold; AHPmedium – medium afterhyperpolarizing potential following a single action potential with a latency of 10-40 ms; AHPslow - slow afterhyperpolarizing potentials, i.e. hyperpolarization following a train of actions potential measured from threshold; ADP - afterdepolarization, small positive deflection in membrane potential following the AHPfast, measured from AHPfast; Statistical significance was computed using the Mann-Whitney-U-Test (n.s. – not significant).

YFP+

	PVP-dendrite	no PVP-dendrite	stria cell	p value
V_M (mV)	–61.5 ± 8.9	–64.3 ± 7.7	–53.8 ± 5.5	<0.01
R_{IN} (MΩ)	805.8 ± 305.0	866.3 ± 516.3	1226.3 ± 442.1	n.s.
τ (ms)	66.13 ± 23.91	55.41 ± 22.43	58.86 ± 24.19	n.s.
C_M (pF)	80.43 ± 37.58	66.23 ± 23.13	39.20 ± 18.74	<0.01
Sag index (%)	2.3 ± 2.5	3.8 ± 5.7	5.9 ± 5.6	n.s.
AHP_{slow} (mV)	0.6 ± 2.5	–1.9 ± 1.6	–3.1 ± 3.8	<0.01
f_{inst} (Hz)	195.6 ± 70.1	216.5 ± 72.0	209.1 ± 63.5	n.s.
$f_{200\ pA}$ (Hz)	62.5 ± 17.1	63.0 ± 11.8	77.3 ± 17.2	<0.05
accommodation index (%)	10.0 ± 11.6	15.4 ± 15.2	13.5 ± 15.2	n.s.
number of cells	32 (30 in τ, 26 in C_M)	16	9	

	PVP-dendrite	no PVP-dendrite	stria cell	p value
AP amplitude(mV)	68.5 ± 8.0	69.1 ± 9.9	74.5 ± 6.3	n.s.
AP threshold(mV)	–27.1 ± 4.1	–29.1 ± 3.5	–29.0 ± 4.5	n.s.
AP duration(ms)	0.74 ± 0.12	0.70 ± 0.19	0.59 ± 0.13	n.s.
AHP_{fast}(mV)	–19.7 ± 4.6	–20.1 ± 4.8	–23.3 ± 5.5	n.s.
AHP_{medium} (mV)	–18.3 ± 4.1	–18.9 ± 3.4	–20.3 ± 4.6	n.s.
ADP (mV)	3.5 ± 2.6	3.6 ± 1.8	4.5 ± 3.6	n.s.
ADP present (%)	65,6	57,1	66,7	n.a.
number of cells	32 (30 in AHPfast)	14	9	

Table 8: Summary of active and passive membrane properties and firing properties of different groups of YFP+ cells.

Abbreviations: VM - resting membrane potential; R_{IN} - membrane input resistance; τ - membrane time constant; C_M - cell capacitance; Sag index - degree of slow inward rectification; AHP - afterhyperpolarization following a train of action potentials; f_{INST} - estimated instantaneous firing frequency; $f_{200\ pA}$ - average firing rate in 200 pA stimulation from –65 mV; accommodation index - comparison of the interspike intervals from the middle and the end of a train of action potentials elicited by 500 ms of 200 pA stimulation; AP - action potential; AP threshold - membrane potential where the slope of the AP equals 20 mV/ms; AHPfast - fast afterhyperpolarizing potential hyperpolarization immediately following the peak of the AP measured from threshold; AHPmedium – medium afterhyperpolarizing potential following a single action potential with a latency of 10-40 ms; AHPslow - slow afterhyperpolarizing potentials, i.e. hyperpolarization following a train of actions potential measured from threshold; ADP - afterdepolarization, small positive deflection in membrane potential following the AHPfast, measured from AHPfast; Statistical significance was computed using the Kruskal-Wallis-Test (n.s. – not significant).

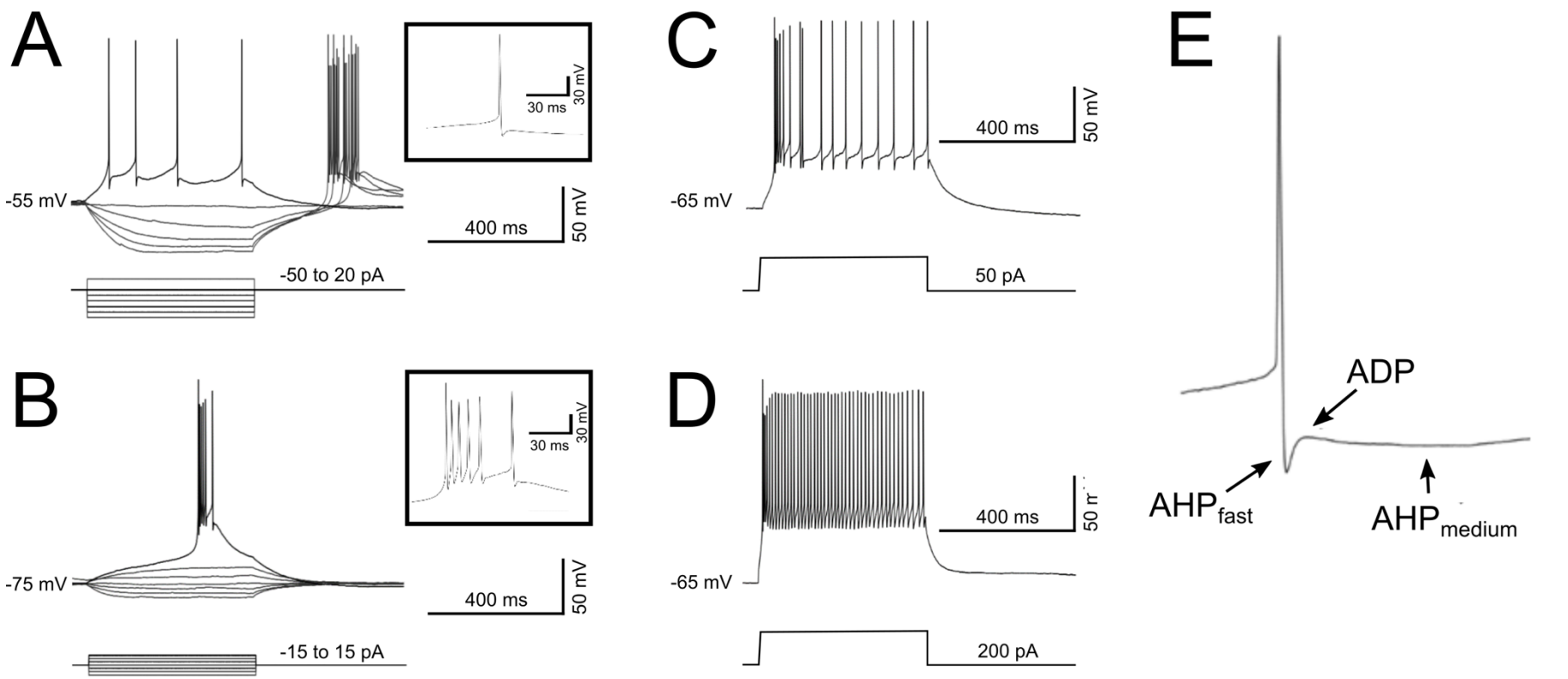

Figure 15: Electrophysiological properties of a YFP+ neuron in the habenula.

A: Voltage responses to hyper- and depolarizing current pulses with holding potential at –55 mV. A single action potential is shown on the right on enlarged time scale. Note, just a regular single spike pattern appears after the depolarizing current injection then burst firing after the end of hyperpolarizing current injections. Furthermore, the more negative current was injected, the faster the voltage response reached a steady state voltage indicating fast inward rectification. **B:** Voltage responses to hyper- and depolarizing current pulses with holding potential at –75 mV. Note, the 15 pA current injection results in a bursting firing pattern, shown with enlarged time scale on the right. **C, D:** Voltage responses to 50 (C) and 200 pA (D) current pulses. On strong stimulation, the firing frequency can be as fast as 90 Hz. **E:** Close-up of a single action potential to illustrate the definition of AHPfast, AHPslow, and ADP.

Abbreviations: ADP - afterdepolarization potential; AHP - afterhyperpolarization potential.

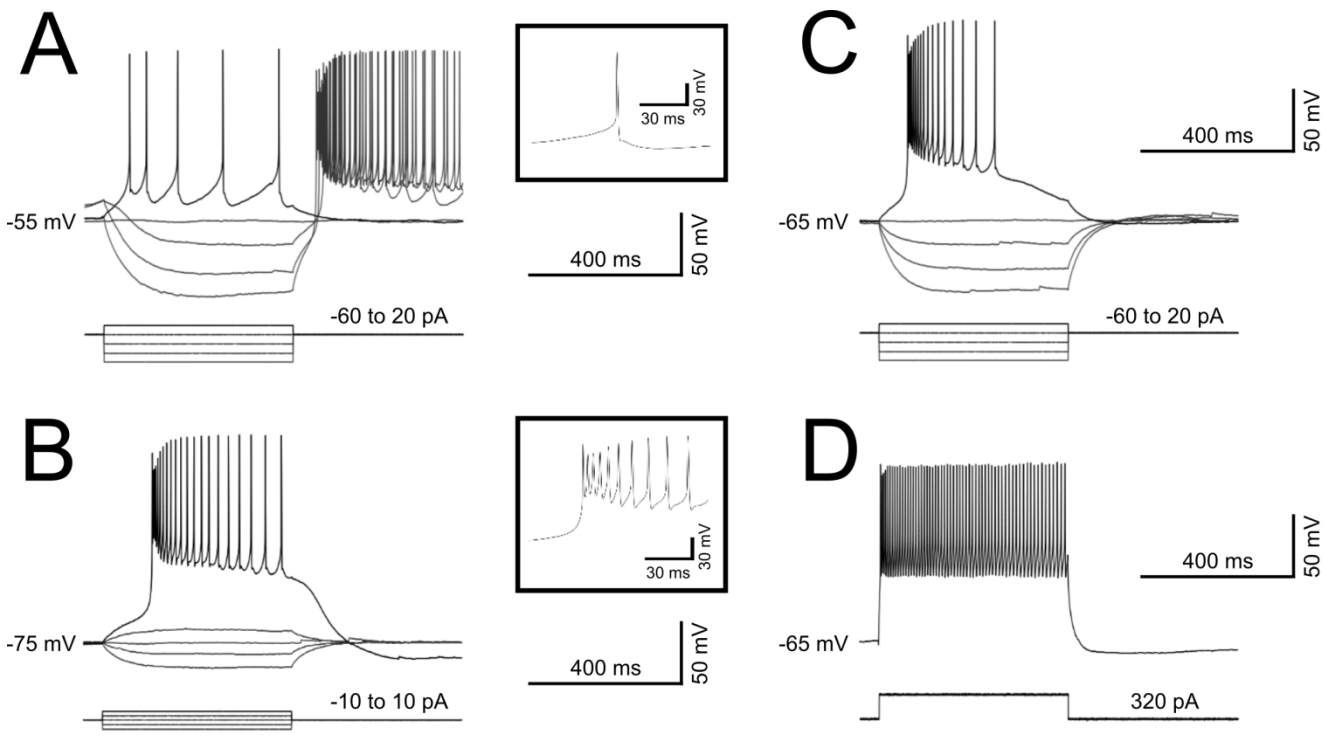

Figure 16: Electrophysiological properties of a YFP– neuron in the habenula.

A: Voltage responses to hyper- and depolarizing current pulses with holding potential at –55 mV. A single action potential is shown on the right with enlarged time scale. Note, just a regular single spike pattern appears after the depolarizing current injection then burst firing after the end of hyperpolarizing current injections. The burst response triggered sustained firing, typically observed in YFP–neurons. **B:** Voltage responses to hyper- and depolarizing current pulses with holding potential at –75 mV. Note, the 10 pA current injection results in a prominent bursting firing pattern, shown with an enlarged time scale on the right. **C, D:** Voltage responses to 20 (C) and 320 pA (D) current pulses. Upon strong stimulation the cell firing frequency was as high as 61 Hz.

5.6 Extracellular stimulation of YFP+ neurons in the LHb

Via the fiber tract of the *stria medullaris (sm*), inputs from different regions of the forebrain reach the habenula. In recent studies it was found that LHb cells are primarily innervated by glutamatergic fibers, but also GABAergic transmission occurs, sometimes even from the same synapse as co-transmission (Shabel et al. 2014).

To determine the input on YFP+ cells, we performed extracellular electrical stimulation of the *stria medullaris* and paraventricular thalamus while recording a neuron in whole-cell mode. The responses were measured at a holding potential of −55 mV in voltage clamp, and the response to two pharmacological agents, DNQX and gabazine, was tested to evaluate the receptors involved in transmission. DNQX is an antagonist of AMPA-type glutamate receptors and thus blocks fast excitatory transmission. Gabazine can be used to block the effect of GABA on GABA-A and GABA-C receptors that usually provide fast ionotropic inhibition to the postsynaptic cell.

Six cells stimulated from the *stria medullaris* and seven cells stimulated from the PVP had a stable series resistance (R_S) during recording and were taken for this analysis.

Stria medullaris

Six cells received fast synaptic input with an average stimulus-to-peak latency of 2.9 ± 0.9 ms and a decay time constant of 3.5 ± 1.3 ms. The average amplitude of the postsynaptic current (PSC) was −69.5 ± 33.0 pA and showed no facilitation when the stimuli were applied in quick succession (paired stimulus, paired pulse ratio, PPR 1.15 ± 0.20). Transmission was reliable with a rate of 91 ± 7% - i.e., failures occurred at less than 10% probability.

The response to pharmacological agents was heterogenous (Fig. 17 B): In 2 cells the administration of DNQX blocked the EPSCs completely (mean amplitude control: −57.6 ± 8.4 pA; mean amplitude DNQX: −6.4 ± 0.5 pA). In 3 cells the administration of DNQX uncovered an IPSC and the addition of gabazine was required to block synaptic transmission completely (mean amplitude control: −81.4 ± 53.0 pA; mean amplitude DNQX: −26.4 ± 4.5 pA; mean amplitude DNQX + gabazine: −11.2 ± 3.6 pA). In one neuron only an IPSC could be elicited. This was completely blocked by gabazine (amplitude control: −57.5 pA; amplitude gabazine: −5.0 pA) These inward, gabazine-sensitive currents could be reversed by applying a more positive holding potential. The reversal

potential of these synaptic events was found to be around −50 mV (Fig. 17E), consistent with a GABA-A receptor-mediated inhibitory transmission.

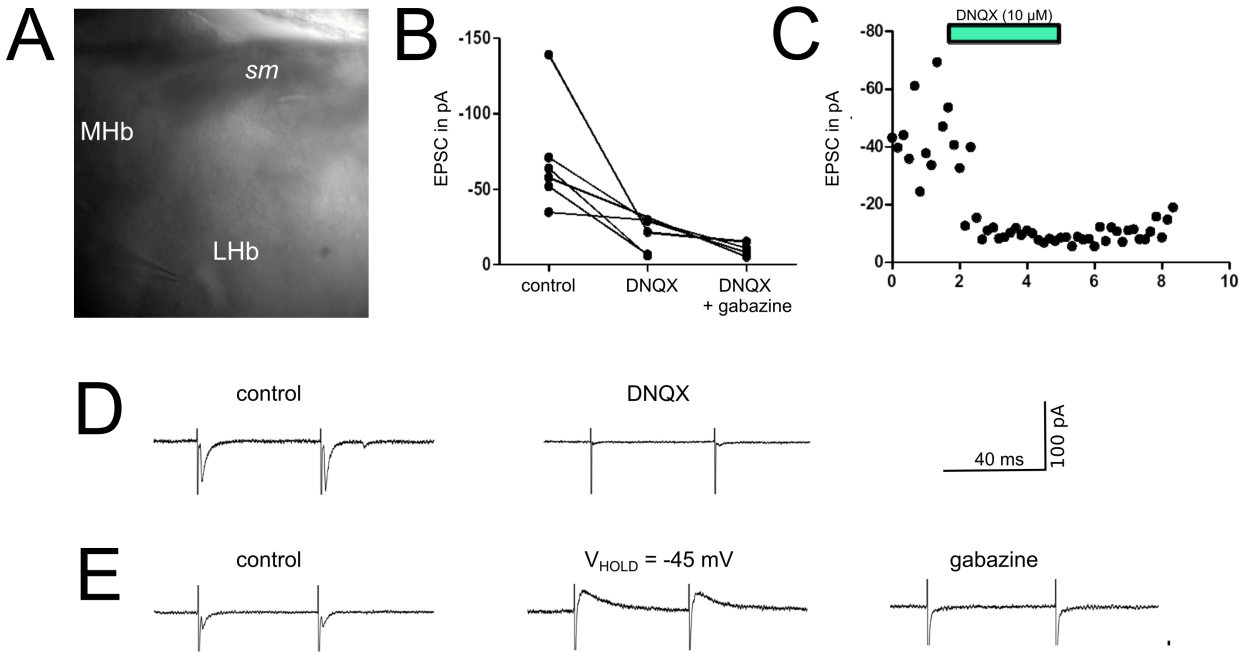

Figure 17: Stimulation in the *stria medullaris (sm)* results in fast glutamatergic and GABAergic transmission.

A: Image of light-microscopy showing the recording electrode in the LHb and the stimulation electrode in the *sm.* **B:** Average amplitudes of PSCs in 6 YFP+ cells with the effects of DNQX and gabazine. **C:** Summary of responses of two YFP+ cells at a holding potential of −55 mV, showing that DNQX blocks inward currents (only means shown). **D:** fast EPSC in a YFP+ cell, which is blocked by DNQX. **E:** Fast inward current with a reversal potential between −55 and −45 mV, which is blocked by gabazine consistent with GABA-A receptor-mediated inhibitory transmission.

Abbreviations: MHb - medial habenula; LHb - lateral habenula.

Posterior paraventricular thalamic nucleus (PVP)

Of the 7 YFP+ cells that were evaluated for input from the PVP, all showed a dendrite extending into this nucleus in the morphological analysis. Six of them were located in the cell group near the paraventricular thalamic nucleus (compare Fig. 7). Fast PSCs were recorded in response to two extracellular stimuli with 50 ms intervals in all of the cells. The average latency was 4.6 ± 1.3 ms, with a decay time constant of 4.6 ± 1.5 ms. The average amplitude of the PSCs was negative in all of the cells and the mean amounted to −39.9 ± 17.8 pA. The second PSC evoked by the paired stimulus was found to be slightly larger on average, with a PPR of 1.22 ± 0.39.

Similar to the results of stimulation in the *stria medullaris*, the response to DNQX and gabazine was heterogenous. In 4 cells the fast PSC was completely blocked by DNQX, indicating fast synaptic transmission via glutamatergic AMPA-type receptors (mean amplitude control: −41.4 ± 22.1 pA; mean amplitude DNQX: −3.2 ± 4.1 pA). One of these cells showed simultaneous slower inhibitory synaptic transmission, with a latency of 11.7 ms and a time constant of 13.7 ms (Fig. 18E). The amplitude of the IPSC was small and could be blocked completely by gabazine (amplitude DNQX: 24.3 pA; amplitude DNQX + gabazine: −11.4 pA).

In 2 neurons, the administration of gabazine resulted in a marked increase of the amplitude of the EPSC (Fig. 18B and C), indicating the presence of an underlying IPSC. The transmission could be blocked completely by the addition of DNQX (mean amplitude control: −32.2 ± 22.1 pA; mean amplitude gabazine: −86.8 ± 34.2 pA; mean amplitude gabazine + DNQX: −10.4 ± 3.2 pA). In the last cell, the administration of DNQX marginally decreased the amplitude of the EPSC, whereas the addition of gabazine blocked synaptic transmission completely (amplitude control: −44.5 pA; amplitude DNQX: −29.7 pA; amplitude DNQX + gabazine: 2.0 pA). This was similar to the transmission in one cell observed during the stimulation of the stria medullaris (Fig. 18E) and is consistent with a GABA-A receptor-mediated inhibitory transmission.

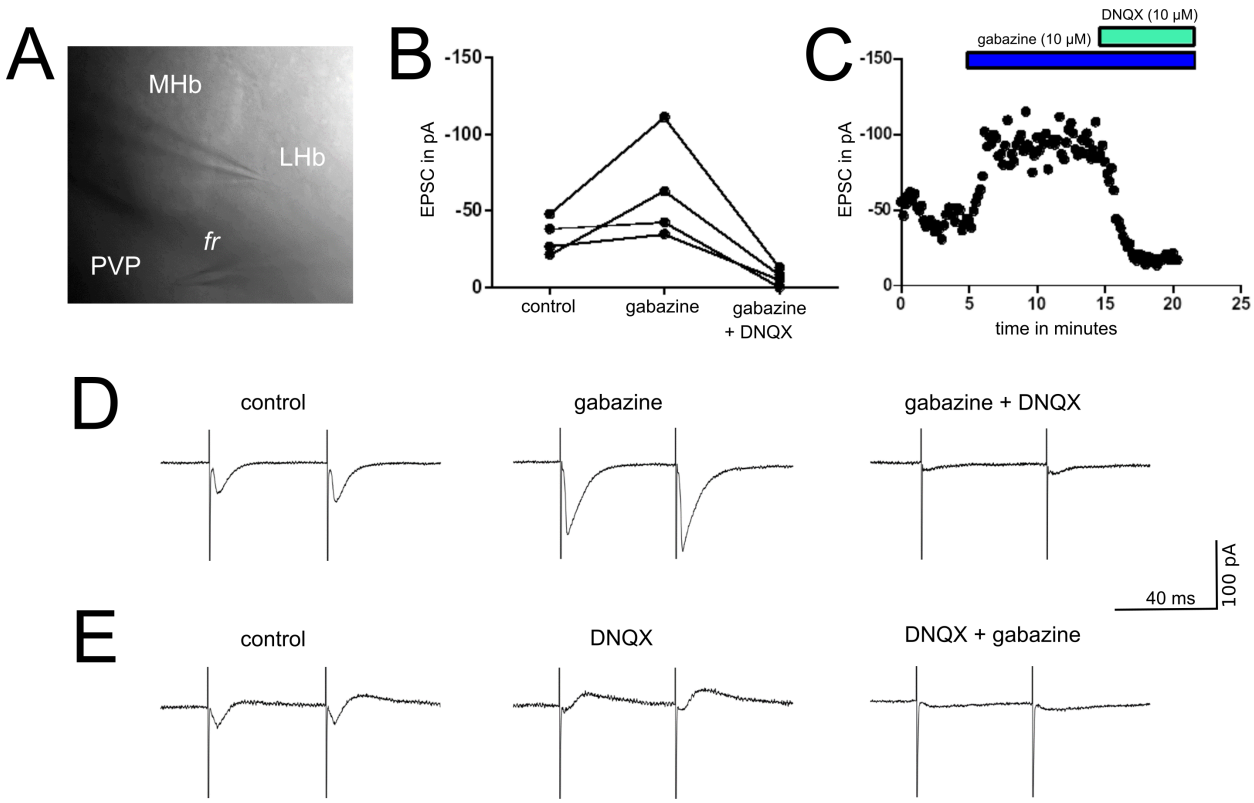

Figure 18: Stimulation in the Posterior Paraventricular Thalamus (PVP) results in both fast glutamatergic and GABAergic transmission.

A: Light-microscopic image showing the patching electrode in the LHb and the stimulation electrode in the PVP. **B:** Average amplitudes of PSCs in 4 YFP+ cells. In two cells the EPSC is augmented by gabazine. **C:** Summary of responses of two YFP+ cells, showing that EPSC amplitudes could be enlarged with gabazine and blocked by DNQX. **D:** Fast EPSC observed in a YFP+ cell, which was augmented by gabazine and blocked by DNQX. **E:** Fast EPSC blocked by DNQX and slower IPSC blocked by gabazine.

Abbreviations: *fr – fasciculus retroflexus;* MHb – medial habenula; LHb – lateral habenula; PVP – posterior paraventricular thalamus.

6 Discussion

The aim of this study was to investigate the identity and characteristics of YFP+ neurons in the lateral habenula of the VGAT-Venus-A transgenic rat. In these animals, we consistently found a population of YFP+ neurons located in the medial part of the LHb and characterized them in terms of electrophysiology and morphology. In contrast to cortical YFP+ cells, however, the population of YFP+ neurons in the LHb did not express GAD67 and did not show any locally branching axon. Thus, they are likely to be projection neurons rather than GABAergic interneurons. Nonetheless, these YFP+ neurons clearly differed from their YFP− counterparts in terms of their morphology and electrophysiology.

6.1 Methodological considerations

One aim of our study was to characterize the morphology of YFP+ neurons in the LHb. A traditional method to study the morphology of neurons is Golgi's method which uses silver salts to stain the cell body and neural excrescences. Several improvements have been made over time and it provides detailed information about the ramification of the dendritic tree and the axon and offers resolution for light and electron microscopy (Vints et al. 2019). A major downside of this methods is that labeling is not specific, i.e., it would not have been restricted to YFP+ neurons in the LHb. Furthermore, labeled neurons often overlap making the analysis of the entire dendritic arbor and the local axon often very difficult or even impossible. Also modern imaging methods such as fluorescence light-sheet-microscopy combined with expansion microcopy have this limitation (Murakami et al. 2018).

Therefore, we chose single-cell labeling with neurobiocytin by filling the cells during patch-clamp experiments using a transgenic rat line expressing a cellular level fluorescent marker. This method allowed for the target and visualization of the neurons using avidin coupled to a fluorescent dye and the subsequent 3D-reconstruction of the recorded neurons with high detail in isolation. A further major advantage is that it allows for the targeted combined physiological and morphological characterization of the cells of interest. A disadvantage of this method is that it is a rather laborious approach and only a small number of neurons can be visualized per experiment. Furthermore, the neurons loose some of their dendrites and axon due to the slicing procedure and require optimization of the slicing procedure, in particular with respect to cutting angle.

As a standard, 300 µm thick coronal slices were used and the axon of the projection neurons was usually cut at the ventral or dorsal surface of the slice. Thus, the axon could not be followed to its remote projection target. We tried to circumvent this problem by using sagittal slices, but in this experiment in 5 rats no YFP+ neurons in the LHb could be visualized by fluorescence microscopy. This was due to the ventro-caudal preferential distribution of these cells along a small corridor at the border with the medial habenula (compare Fig. 6). This makes it very hard to obtain slices containing this small corridor near the surface of the slice and accessible to the micropipette. In other studies of the LHb sagittal slices have been used, but without targeting a specific population of neurons (Li et al. 2011).
As our primary aim was to evaluate the presumed local arborization of the axon, we therefor returned to coronal slices where the yield of YFP+ neurons during the experiments was much higher.

To evaluate the synaptic input to YFP+ neurons in the LHb, we performed extracellular electrical stimulation of the *stria* medullaris and the paraventricular thalamus. This allowed for local stimulation of fiber tracts and electrical stimulation has been used to study synaptic transmission in the LHb via the *stria medullaris* (Li et al. 2011) and in other parts of the diencephalon such as the subthalamic nucleus (Amadeus Steiner et al. 2019). In extracellular stimulation the excitation of fibers is not specific, but it has long been the standard in the evaluation of synaptic responses and with the use of a minimal stimulation paradigm even single axons can be activated (Glasgow et al. 2019).
Since 2005 photostimulation using optogenetics has gained more and more attention as a versatile tool to study neuronal connectivity by stimulation of the somata or the fiber tracts itself (Yizhar et al. 2011) and has also been successfully employed in studies of the LHb (overview in Biselli et al. 2019; Shabel et al. 2014). Light-sensitive proteins are introduced into the cell membrane of the neuron and allow cell type-specific manipulation of the neurons, such as the generation of action potentials or the activation of G protein-coupled receptors (Deisseroth 2011).
One advantage over conventional electrical stimulation is its specificity, i.e., the light impulse can target only a predefined subset of neurons. This better resembles the asynchronous firing in neural networks (Deisseroth 2011; Glasgow et al. 2019).

On the other hand, stimulation using optogenetics requires the injection of a viral vector into the target region or the knowledge of a well-defined group of presynaptic neurons to create a transgenic animal expressing the optogene together with a neuronal marker. These techniques require a significant amount of operating expense. This was not possible in the current project.
In conclusion, electrical stimulation using a microelectrode was a more practical choice to us in the study of the synaptic transmission on YFP+ neurons.

One goal of this study was to find out, if YFP+ neurons in the LHb are GABAergic cells. There is a diversity of markers for the identification of GABAergic neurons in the brain (Tremblay et al. 2016). The protein VGAT is a major and specific marker of GABAergic neurons in the central nervous system. VGAT is necessary for the transport of GABA into the synaptic vesicles and thus is present in all GABAergic neurons (Gasnier 2000). In fact, the reporter fluorescent protein was expressed under the promotor of VGAT in the transgenic line. Therefore, we aimed at obtaining independent evidence for the GABAergic nature of the cells by other markers.
The small molecule GABA, which acts as the inhibitory neurotransmitter, itself can be detected by immunohistochemistry, but its content varies significantly between different types of neurons and is present in lower concentrations in all neurons as a product of glutamate metabolism (Jinno et al. 1998).
The enzymes GAD65 and GAD67 catalyze the conversion of glutamic acid to GABA and are present in GABAergic cells at variable levels (Erlander and Tobin 1991). Because GAD67 is the prominent enzyme in the cytoplasm of GABAergic neurons, we chose this isoform for our *in situ* hybridization experiments.
Taken together there is no single marker for GABAergic neurons. The strategies of labeling that are used for cortical interneurons, which includes the labeling of calcium-binding proteins such as parvalbumin might not be as reliable and consistent in the diencephalon compared to the cortex.

6.2 Evidence of GABAergic interneurons in the LHb

Even in the most recent literature the existence of GABAergic interneurons in the LHb remains a debated issue. Recent evidence suggests that there is a small number of GABAergic interneurons in the LHb of rats. First, Wagner et al. demonstrated a small number of GAD67 positive neurons in the medial part of the LHb (Wagner et al. 2016). In addition, the group of Zhang et al. showed cells in the medial part of the LHb of male rats that exhibit an extensively branching axon in the LHb and were labeled for both VGAT and GAD65 as well as for the estrogen receptor α (ERα) (L. Zhang et al. 2018; Zhang and Hernández 2016). Only 6 cells were reported, but in situ hybridization showed a larger number of neurons with positive labeling for both GAD65 and ERα. These cells fulfil criteria of interneuron morphology. They were located along the border of the medial and the lateral habenula, just like the majority of neurons in our study (compare Fig. 14). Notably, the number of these neurons differed markedly depending on the hormone status of the animal (L. Zhang et al. 2018).

This is in contrast to previous experiments and our study findings that showed GABAergic neurons to be located almost exclusively in the lateral part of the LHb (Brinschwitz et al. 2010). Thus, it is likely that despite the overlapping localization, the YFP+ neurons and the GABAergic interneurons studied by Zhang et al. form different neuronal populations. Phenotype switching, i.e. that neurons change their primary neurotransmitter, is a validated concept in neuroscience (Spitzer 2015) and has been demonstrated in dentate gyrus cells in the hippocampus (Gutiérrez 2002). As we used adolescent animals for our *in vitro* experiments, the number of GABAergic cells might have been lower, but it is important to note in this context, that in our sample no extensive axon branching could be observed. Ultimately it remains to be elucidated if YFP+ neurons in the LHb express the ERα and might indeed overlap with the population of cells described by Zhang et al.

A recent study demonstrated a small number of GABAergic neurons co-labeled for parvalbumin in the lateral habenula of transgenic mice. Photostimulation of these PV-positive neurons elicited IPSPs in a low number of neurons in the oval subnucleus of the LHb, indicating local inhibitory transmission via GABA-A receptors (Webster et al. 2020). In a set of experiments Quina et al. compared the expression of VGAT, GAD65 (GAD2 as the encoding gene) and GAD67 (GAD1 as the encoding gene) in neurons in the LHb using fluorescent *in situ* hybridization. They found distinct subgroups of neurons in

agreement with our study results, but no cells were labeled for all three markers. This implies that GABAergic cells are absent in the LHb. This notion is further supported by the positive labeling against the vesicular glutamate transporter 2 (VGLUT2) found in neurons labeled for GAD1/GAD67 (Quina et al. 2020). Interestingly, as a further aspect, differences in the expression of VGAT, GAD65 and GAD67 between rat and mouse were observed in this study, questioning the comparability of studies of the LHb carried out in these two species.

In our study, we explored the distribution of neurons expressing parvalbumin and calbindin which are calcium-binding proteins expressed in subsets of cortical interneurons. In our samples only a small number of YFP+ neurons expressed calbindin and there was no overlap with PV-positive cells. Webster et al. described a small number of neurons in the lateral part of the LHb that expressed both PV and VGAT, whereas the PV-positive neurons in the medial part did not label for VGAT(Webster et al. 2020). However, the latter experiments were carried out in mice and one explanation for this discrepancy could be the differential expression of these neuronal markers in the two species (see above).

In conclusion, the available evidence argues against the existence of a significant population of GABAergic interneurons in the LHb of the rat, but further studies are necessary to settle this controversial question.

6.3 Identity of YFP+ cells in the LHb

We showed that YFP+ cells could be clearly distinguished from their YFP− counterparts based on their passive membrane properties and the absence of sustained firing after a burst response. This hyperpolarization-induced bursting followed by a long train of action potentials has been described as a hallmark of glutamatergic neurons in the LHb (Chang and Kim 2004). The distinction was further supported by the finding that the axons of YFP+ cells preferentially did not join the *fasciculus retroflexus,* as was the case for all YFP− cells. In addition, a subgroup of YFP+ neurons showed a dendritic tuft in the neighboring paraventricular thalamus. This feature was not observed in any of the YFP−

cells, including those recorded in the region near the medial habenula. Overall, the characteristics of YFP− cells in this study were in good agreement with previous work on neurons in the LHb (Weiss and Veh 2011).
Therefore, YFP+ neurons in the LHb seem to constitute a distinct entity, and different explanations might be offered to explain our findings:

(1) YFP+ neurons are a population that is not found in non-transgenic animals, and the transgene accounts for their altered properties in comparison to YFP− cells, which were clearly documented in this study. This is highly unlikely, however, because numerous other studies have shown that BAC-inserted technology does not alter the properties and identity of neurons (Heintz 2001; Meyer et al. 2002). In addition, the labeling for VGAT using *in situ* hybridization was in good agreement with the distribution of VGAT-YFP+ cells in our study, with most of the neurons located in the medial part of the LHb (Quina et al. 2020) and a study using VGluT2-GAD and VGluT2-VGAT transgenic rats observed no co-localization of GAD and VGAT in the LHb (Root et al. 2018).

(2) YFP+ neurons are a population that also exists in non-transgenic animals and are labeled despite not being genuine GABAergic interneurons - i.e., mis-expression. This is suggested by comparison with the other VGAT-Venus strain B, which does show very minor labeling in both the LHb and the thalamus. VGAT, and consequently YFP, might be aberrantly expressed in these neurons, most likely due to a positional effect of the BAC-inserted transgene (Uematsu et al. 2008). However, this is in contrast with the aforementioned findings by Quina et al. that showed VGAT-expression in the medial part of the LHb in the rat but no labeling for other markers of GABAergic cells.

(3) YFP+ neurons use glycine as a neurotransmitter, since VGAT also serves for the transport of glycine into vesicles. Glycine is present primarily in interneurons of the brainstem and the spinal cord, but a small number of immunoreactive neurons was also found in the lateral habenula and subfornical region (Rampon et al. 1996), and the injection of glycine into the LHb reduced alcohol intake in rats experiencing alcohol withdrawal (Li et al. 2019).

(4) YFP+ neurons are glutamatergic projection neurons that use GABA as a co-transmitter. This has been shown in cells from the basal ganglia providing input to the habenula via the *stria medullaris* (Shabel et al. 2014). With GABA not being the primary neurotransmitter, the content of GAD-67 might have been too low to yield positive labeling in the *in situ* hybridization.

6.4 Groups of YFP+ neurons

Within the population of YFP+ cells in the LHb, three groups could be distinguished based on their morphology and location. The group of cells in the *stria medullaris* was comprised of small neurons with their cell bodies intercalated between the fiber tracts. The group of neurons without a dendritic tuft in the PVP was very similar to the population of YFP-neurons and could be distinguished only based on electrophysiology.

The group of cells with a dendritic tuft in the PVP was the most interesting. These neurons showed extensive branching of their dendritic tree in the neighboring posterior paraventricular nucleus of the thalamus and received glutamatergic as well as GABAergic input from this brain region. This is one of few examples of dendrites crossing specified anatomical borders of well-defined brain structures (Walker et al. 1993).

The paraventricular thalamus is one of the thalamic structures that comprise the midline thalamus and has been assigned an important role in stress responses, anxiety and food- as well as drug-seeking behavior (Hsu et al. 2014). Moreover, the paraventricular thalamus was shown to influence wakefulness via a connection with the nucleus accumbens (Ren et al. 2018).This is supported by the finding of a heavy innervation from the hypothalamus, in particular with fibers containing neuropeptides such as orexin and from limbic cortical areas such as the prelimbic and posterior insular cortex (Colavito et al. 2015; Li and Kirouac 2012). In the rat, one major projection target of neurons of the PVP is the central nucleus of the amygdala that is thought to play a major role in fear expression and learning (Penzo et al. 2015). But PVP neurons can also enhance dopamine release in the shell of the *nucleus accumbens* independently of the VTA, regulating the dopamine levels in parts of the striatum similar to the LHb (Parsons, Li, and Kirouac 2007) and have been shown to regulate behavior under motivational conflict (Choi et al. 2019).

In our experiments, the YFP+ neurons with a PVP-dendrite are the first evidence of a direct communication between the thalamus and the lateral habenula, although due to their scarce number their functional relevance remains unclear.

Another interesting feature of this group of YFP+ neurons was the course of their axon. It was highly variable, and the rostral course of the axon in a subset of YFP+ cells could indicate a backward projection of LHb neurons through the *stria medullaris* to regions in the forebrain. Unfortunately, we failed to prove this in sagittal slices because of the scarce number of YFP+ cells. Further experiments using *in vivo* patch-clamp or antegrade tracing could help to clarify the projection targets of these neurons.
While a possibility is, that neurons recorded near the thalamic border were thalamic cells, due to the clear border of the *fasciculus retroflexus* and the larger cell bodies of thalamic neurons visible in light microscopy, we consider this possibility as highly unlikely.

6.5 Synaptic inputs to YFP+ neurons

Extracellular stimulation of the *stria medullaris* revealed both glutamatergic input via AMPA-receptors as well as GABAergic input via GABA-A receptors acting on YFP+ cells. Stimulation experiments were only conducted in a minority of YFP+ cells, and in half of these this input occurred simultaneously with a short latency, suggesting monosynaptic transmission. Research using optogenetic stimulation of fibers of the *sm* has shown that glutamate and GABA are co-released from synapses of striatal projection neurons onto LHb neurons (Shabel et al. 2014). That research was confined to the lateral part of the LHb, whereas the YFP+ neurons evaluated in this work were located exclusively in the medial part of the LHb. Nonetheless, the same mechanisms of co-release might be present at synapses converging onto YFP+ as for YFP- ones. However, when analyzing on the single cell level, we found a large variability: in only a subset of the cells was both a glutamatergic and a GABAergic response observed in response to stimulation. In other cells either EPSCs or IPSCs were elicited, suggesting that distinct populations of presynaptic axons mediate excitatory and inhibitory synaptic effects onto these cells.
Qualitatively similar results were obtained in neurons with a dendritic tuft in the PVP in response to stimulation in the PVP - mixed and variable glutamatergic and GABAergic transmission was observed. Interestingly, a comparable proportion of the neurons received glutamatergic and GABAergic inputs, which is surprising given the low number

of GABAergic cells in the thalamic nuclei. The GABAergic input is therefore likely to originate from outside the PVP, for example in the reticulate thalamic nucleus.

6.6 Conclusion

In summary YFP+ neurons form a distinct entity of cells in the LHb, but exhibit features of projection neurons, rather than inhibitory interneurons. This is supported by the absence of GAD67 and the lack of expression of calcium-binding proteins, as well as by their morphological features, most prominently the non-branching axon. Recent research has demonstrated the existence of a small number of GABAergic interneurons in the LHb, but their relation to cells examined in this study remains open. YFP+ cells receive excitatory as well as inhibitory input from the *stria medullaris* and the paraventricular thalamic nucleus. The precise identity of these cells, as well as the functional relevance of their connection to the thalamus, remain to be elucidated.

7 References

Aizawa, Hidenori, Ryunosuke Amo, and Hitoshi Okamoto. 2011. “Phylogeny and Ontogeny of the Habenular Structure.” *Frontiers in Neuroscience* 5. doi: 10.3389/fnins.2011.00138.

Aizawa, Hidenori, Megumi Kobayashi, Sayaka Tanaka, Tomoki Fukai, and Hitoshi Okamoto. 2012. “Molecular Characterization of the Subnuclei in Rat Habenula.” *The Journal of Comparative Neurology* 520(18):4051–66. doi: 10.1002/cne.23167.

Amadeus Steiner, Leon, Federico J. Barreda Tomás, Henrike Planert, Henrik Alle, Imre Vida, and Jörg R. P. Geiger. 2019. “Connectivity and Dynamics Underlying Synaptic Control of the Subthalamic Nucleus.” *The Journal of Neuroscience* 1642–18. doi: 10.1523/JNEUROSCI.1642-18.2019.

Arcelli, P., C. Frassoni, M. C. Regondi, Dipartimentodi Neurofisiologia, Dipattimentodi Fisiologiae Biochimicagenerali, Sezionedi Istologiae, and Anatomia Umana. 1997. “GABAergic Neurons in Mammalian Thalamus: A Marker of Thalamic Complexity?” 42(1):27–37.

Bernard, René, and Rüdiger W. Veh. 2012. “Individual Neurons in the Rat Lateral Habenular Complex Project Mostly to the Dopaminergic Ventral Tegmental Area or to the Serotonergic Raphe Nuclei.” *The Journal of Comparative Neurology* 520(11):2545–58. doi: 10.1002/cne.23080.

Biselli, Tom, Susen Sophie Lange, Lynn Sablottny, Johannes Steffen, and Andreas Walther. 2019. “Optogenetic and Chemogenetic Insights into the Neurocircuitry of Depression-like Behaviour: A Systematic Review.” *European Journal of Neuroscience*. doi: 10.1111/ejn.14603.

Boku, Shuken, Shin Nakagawa, Hiroyuki Toda, and Akitoyo Hishimoto. 2018. “Neural Basis of Major Depressive Disorder: Beyond Monoamine Hypothesis.” *Psychiatry and Clinical Neurosciences* 72(1):3–12. doi: 10.1111/pcn.12604.

Booker, S. A., A. Gross, D. Althof, R. Shigemoto, B. Bettler, M. Frotscher, M. Hearing, K. Wickman, M. Watanabe, A. Kulik, and I. Vida. 2013. “Differential GABAB-Receptor-Mediated Effects in Perisomatic- and Dendrite-Targeting Parvalbumin Interneurons.” *Journal of Neuroscience* 33(18):7961–74. doi: 10.1523/JNEUROSCI.1186-12.2013.

Brinschwitz, K., A. Dittgen, V. I. Madai, R. Lommel, S. Geisler, and R. W. Veh. 2010. “Glutamatergic Axons from the Lateral Habenula Mainly Terminate on GABAergic Neurons of the Ventral Midbrain.” *Neuroscience* 168(2):463–76. doi:

10.1016/j.neuroscience.2010.03.050.

Bromberg-martin, Ethan S., Okihide Hikosaka, and Kae Nakamura. 2010. “Coding of Task Reward Value in the Dorsal Raphe Nucleus.” 30(18):6262–6272. doi: 10.1523/JNEUROSCI.0015-10.2010.

Bromberg-martin, Ethan S., Masayuki Matsumoto, and Okihide Hikosaka. 2010. “Dopamine in Motivational Control: Rewarding, Aversive, and Alerting.” *Neuron* 68(5):815–834. doi: 10.1016/j.neuron.2010.11.022.

Chang, Su-youne, and Uhnoh Kim. 2004. “Ionic Mechanism of Long-Lasting Discharges of Action Potentials Triggered by Membrane Hyperpolarization in the Medial Lateral Habenula.” 24(9):2172–2181. doi: 10.1523/JNEUROSCI.4891-03.2004.

Choi, Eun A., Philip Jean-Richard-dit-Bressel, Colin W. G. Clifford, and Gavan P. McNally. 2019. “Paraventricular Thalamus Controls Behavior during Motivational Conflict.” *The Journal of Neuroscience* 39(25):4945–58. doi: 10.1523/JNEUROSCI.2480-18.2019.

Cohen, Jeremiah Y., Mackenzie W. Amoroso, and Naoshige Uchida. 2015. “Serotonergic Neurons Signal Reward and Punishment on Multiple Timescales.” *ELife* 4. doi: 10.7554/eLife.06346.

Colavito, Valeria, Chiara Tesoriero, Amenu T. Wirtu, Gigliola Grassi-Zucconi, and Marina Bentivoglio. 2015. “Limbic Thalamus and State-Dependent Behavior: The Paraventricular Nucleus of the Thalamic Midline as a Node in Circadian Timing and Sleep/Wake-Regulatory Networks.” *Neuroscience and Biobehavioral Reviews* 54:3–17. doi: 10.1016/j.neubiorev.2014.11.021.

Deisseroth, Karl. 2011. “Optogenetics.” *Nature Methods* 8(1):26–29. doi: 10.1038/nmeth.f.324.

Edelstein, Arthur, Nenad Amodaj, Karl Hoover, Ron Vale, and Nico Stuurman. 2010. “Computer Control of Microscopes Using MManager.” *Current Protocols in Molecular Biology* Chapter 14:Unit14.20. doi: 10.1002/0471142727.mb1420s92.

Erlander, Mark G., and Allan J. Tobin. 1991. “The Structural and Functional Heterogeneity of Glutamic Acid Decarboxylase: A Review.” *Neurochemical Research* 16(3):215–26. doi: 10.1007/BF00966084.

Gasnier, B. 2000. “The Loading of Neurotransmitters into Synaptic Vesicles.” *Biochimie* 82(4):327–37. doi: 10.1016/S0300-9084(00)00221-2.

Geisler, Stefanie, Karl Hermann Andres, and Rüdiger W. Veh. 2003. “Morphologic and Cytochemical Criteria for the Identification and Delineation of Individual Subnuclei within

the Lateral Habenular Complex of the Rat." *Journal of Comparative Neurology* 458(1):78–97. doi: 10.1002/cne.10566.

Glasgow, Stephen D., Ryan McPhedrain, Jeanne F. Madranges, Timothy E. Kennedy, and Edward S. Ruthazer. 2019. "Approaches and Limitations in the Investigation of Synaptic Transmission and Plasticity." *Frontiers in Synaptic Neuroscience* 11. doi: 10.3389/fnsyn.2019.00020.

Gonçalves, Luciano, Chemutai Sego, and Martin Metzger. 2012. "Differential Projections from the Lateral Habenula to the Rostromedial Tegmental Nucleus and Ventral Tegmental Area in the Rat." *The Journal of Comparative Neurology* 520(6):1278–1300. doi: 10.1002/cne.22787.

Gutiérrez, Rafael. 2002. "Activity-Dependent Expression of Simultaneous Glutamatergic and GABAergic Neurotransmission From the Mossy Fibers In Vitro." *Journal of Neurophysiology* 87(5):2562–70. doi: 10.1152/jn.2002.87.5.2562.

Heintz, Nathaniel. 2001. "Bac to the Future: The Use of Bac Transgenic Mice for Neuroscience Research." *Nature Reviews Neuroscience* 2(12):861–70. doi: 10.1038/35104049.

Hikosaka, Okihide. 2010. "The Habenula: From Stress Evasion to Value-Based Decision-Making." *Nature Reviews Neuroscience* 11(7):503–13. doi: 10.1038/nrn2866.

Hsu, David T., Gilbert J. Kirouac, Jon-Kar Zubieta, and Seema Bhatnagar. 2014. "Contributions of the Paraventricular Thalamic Nucleus in the Regulation of Stress, Motivation, and Mood." *Frontiers in Behavioral Neuroscience* 8. doi: 10.3389/fnbeh.2014.00073.

Huang, Lu, Yue Xi, Yanfang Peng, Yan Yang, Xiaodan Huang, Yunwei Fu, Qian Tao, Jia Xiao, Tifei Yuan, Kai An, Huan Zhao, Mingliang Pu, Fuqiang Xu, Tian Xue, Minmin Luo, Kwok-Fai So, and Chaoran Ren. 2019. "A Visual Circuit Related to Habenula Underlies the Antidepressive Effects of Light Therapy." *Neuron* 102(1):128-142.e8. doi: 10.1016/j.neuron.2019.01.037.

Jhou, Thomas C., Stefanie Geisler, Michela Marinelli, Beth A. Degarmo, and Daniel S. Zahm. 2009. "The Mesopontine Rostromedial Tegmental Nucleus: A Structure Targeted by the Lateral Habenula That Projects to the Ventral Tegmental Area of Tsai and Substantia Nigra Compacta." *The Journal of Comparative Neurology* 513(6):566–96. doi: 10.1002/cne.21891.

Jinno, Shozo, Yusuke Aika, Takaichi Fukuda, and Toshio Kosaka. 1998. "Quantitative

Analysis of GABAergic Neurons in the Mouse Hippocampus, with Optical Disector Using Confocal Laser Scanning Microscope." *Brain Research* 814(1–2):55–70. doi: 10.1016/S0006-8993(98)01075-0.

Kim, Uhnoh. 2009. "Topographic Commissural and Descending Projections of the Habenula in the Rat." *The Journal of Comparative Neurology* 513(2):173–87. doi: 10.1002/cne.21951.

Kim, Uhnoh, and Su Youne Chang. 2005. "Dendritic Morphology, Local Circuitry, and Intrinsic Electrophysiology of Neurons in the Rat Medial and Lateral Habenular Nuclei of the Epithalamus." *Journal of Comparative Neurology* 483(2):236–250. doi: 10.1002/cne.20410.

Lecourtier, Lucas, and Peter H. Kelly. 2007. "A Conductor Hidden in the Orchestra? Role of the Habenular Complex in Monoamine Transmission and Cognition." *Neuroscience & Biobehavioral Reviews* 31(5):658–72. doi: 10.1016/j.neubiorev.2007.01.004.

Li, Bo, Joaquin Piriz, Martine Mirrione, ChiHye Chung, Christophe D. Proulx, Daniela Schulz, Fritz Henn, and Roberto Malinow. 2011. "Synaptic Potentiation onto Habenula Neurons in the Learned Helplessness Model of Depression." *Nature* 470(7335):535–39. doi: 10.1038/nature09742.

Li, Kun, Tao Zhao, Lujian Liao, Fritz Henn, Catherine Wong, Roberto Malinow, John R. Yates, and Hailan Hu. 2013. "SSCaMKII in Lateral Habenula Mediates Core Symptoms of Depression." *Science* 341(6149):1012–16. doi: 10.1126/science.1236501.

Li, Sa, and Gilbert J. Kirouac. 2012. "Sources of Inputs to the Anterior and Posterior Aspects of the Paraventricular Nucleus of the Thalamus." *Brain Structure & Function* 217(2):257–73. doi: 10.1007/s00429-011-0360-7.

Li, Wenting, Wanhong Zuo, Wei Wu, Qi Kang Zuo, Rao Fu, Liangzhi Wu, Haifeng Zhang, Michael Ndukwe, and Jiang-Hong Ye. 2019. "Activation of Glycine Receptors in the Lateral Habenula Rescues Anxiety- and Depression-like Behaviors Associated with Alcohol Withdrawal and Reduces Alcohol Intake in Rats." *Neuropharmacology* 157:107688. doi: 10.1016/j.neuropharm.2019.107688.

Matsumoto, Masayuki, and Okihide Hikosaka. 2007. "Lateral Habenula as a Source of Negative Reward Signals in Dopamine Neurons." *Nature* 447(7148):1111–15. doi: 10.1038/nature05860.

Meyer, Axel H., István Katona, Maria Blatow, Andrei Rozov, and Hannah Monyer. 2002. "*In Vivo* Labeling of Parvalbumin-Positive Interneurons and Analysis of Electrical

Coupling in Identified Neurons." *The Journal of Neuroscience* 22(16):7055–64. doi: 10.1523/JNEUROSCI.22-16-07055.2002.

Monti, Jaime M. 2011. "Serotonin Control of Sleep-Wake Behavior." *Sleep Medicine Reviews* 15(4):269–81. doi: 10.1016/j.smrv.2010.11.003.

Murakami, Tatsuya C., Tomoyuki Mano, Shu Saikawa, Shuhei A. Horiguchi, Daichi Shigeta, Kousuke Baba, Hiroshi Sekiya, Yoshihiro Shimizu, Kenji F. Tanaka, Hiroshi Kiyonari, Masamitsu Iino, Hideki Mochizuki, Kazuki Tainaka, and Hiroki R. Ueda. 2018. "A Three-Dimensional Single-Cell-Resolution Whole-Brain Atlas Using CUBIC-X Expansion Microscopy and Tissue Clearing." *Nature Neuroscience* 21(4):625–37. doi: 10.1038/s41593-018-0109-1.

Parsons, Matthew P., Sa Li, and Gilbert J. Kirouac. 2007. "Functional and Anatomical Connection between the Paraventricular Nucleus of the Thalamus and Dopamine Fibers of the Nucleus Accumbens." *The Journal of Comparative Neurology* 500(6):1050–63. doi: 10.1002/cne.21224.

Penzo, Mario A., Vincent Robert, Jason Tucciarone, Dimitri De Bundel, Minghui Wang, Linda Van Aelst, Martin Darvas, Luis F. Parada, Richard D. Palmiter, Miao He, Z. Josh Huang, and Bo Li. 2015. "The Paraventricular Thalamus Controls a Central Amygdala Fear Circuit." *Nature* 519(7544):455–59. doi: 10.1038/nature13978.

Quina, Lely A., Andrew Walker, Glenn Morton, Victor Han, and Eric. E. Turner. 2020. "GAD2 Expression Defines a Class of Excitatory Lateral Habenula Neurons in Mice That Project to the Raphe and Pontine Tegmentum." *Eneuro* 7(3):ENEURO.0527-19.2020. doi: 10.1523/ENEURO.0527-19.2020.

Rampon, C., P. H. Luppi, P. Fort, C. Peyron, and M. Jouvet. 1996. "Distribution of Glycine-Immunoreactive Cell Bodies and Fibers in the Rat Brain." *Neuroscience* 75(3):737–55. doi: 10.1016/0306-4522(96)00278-3.

Ren, Shuancheng, Yaling Wang, Faguo Yue, Xiaofang Cheng, Ruozhi Dang, Qicheng Qiao, Xueqi Sun, Xin Li, Qian Jiang, Jiwei Yao, Han Qin, Guanzhong Wang, Xiang Liao, Dong Gao, Jianxia Xia, Jun Zhang, Bo Hu, Junan Yan, Yanjiang Wang, Min Xu, Yunyun Han, Xiangdong Tang, Xiaowei Chen, Chao He, and Zhian Hu. 2018. "The Paraventricular Thalamus Is a Critical Thalamic Area for Wakefulness." *Science* 362(6413):429–34. doi: 10.1126/science.aat2512.

Root, David H., Shiliang Zhang, David J. Barker, Jorge Miranda-Barrientos, Bing Liu, Hui-Ling Wang, and Marisela Morales. 2018. "Selective Brain Distribution and Distinctive

Synaptic Architecture of Dual Glutamatergic-GABAergic Neurons." *Cell Reports* 23(12):3465–79. doi: 10.1016/j.celrep.2018.05.063.

Sartorius, Alexander, Karl L. Kiening, Peter Kirsch, Carl C. von Gall, Uwe Haberkorn, Andreas W. Unterberg, Fritz A. Henn, and Andreas Meyer-Lindenberg. 2010. "Remission of Major Depression under Deep Brain Stimulation of the Lateral Habenula in a Therapy-Refractory Patient." *Biological Psychiatry* 67(2):e9–11. doi: 10.1016/j.biopsych.2009.08.027.

Schlögl, A., P. Jonas, C. Schmidt-Hieber, and S. J. Guzman. 2013. "Stimfit: A Fast Visualization and Analysis Environment for Cellular Neurophysiology." *Biomedizinische Technik. Biomedical Engineering*. doi: 10.1515/bmt-2013-4181.

Schultz, Wolfram, Peter Dayan, and P. Read Montague. 1997. "A Neural Substrate of Prediction and Reward." 8.

Shabel, S. J., C. D. Proulx, J. Piriz, and R. Malinow. 2014. "GABA/Glutamate Co-Release Controls Habenula Output and Is Modified by Antidepressant Treatment." *Science* 345(6203):1494–98. doi: 10.1126/science.1250469.

Shabel, Steven J., Christophe D. Proulx, Anthony Trias, Ryan T. Murphy, and Roberto Malinow. 2012. "Input to the Lateral Habenula from the Basal Ganglia Is Excitatory, Aversive, and Suppressed by Serotonin." *Neuron* 74(3):475–81. doi: 10.1016/j.neuron.2012.02.037.

Soltesz, Ivan. 2006. *Diversity in the Neuronal Machine: Order and Variability in Interneuronal Microcircuits*. Oxford, New York: Oxford University Press.

Spitzer, Nicholas C. 2015. "Neurotransmitter Switching? No Surprise." *Neuron* 86(5):1131–44. doi: 10.1016/j.neuron.2015.05.028.

Tremblay, Robin, Soohyun Lee, and Bernardo Rudy. 2016. "GABAergic Interneurons in the Neocortex: From Cellular Properties to Circuits." *Neuron* 91(2):260–92. doi: 10.1016/j.neuron.2016.06.033.

Uematsu, M., Y. Hirai, F. Karube, S. Ebihara, M. Kato, K. Abe, K. Obata, S. Yoshida, M. Hirabayashi, Y. Yanagawa, and Y. Kawaguchi. 2008. "Quantitative Chemical Composition of Cortical GABAergic Neurons Revealed in Transgenic Venus-Expressing Rats." *Cerebral Cortex* 18(2):315–30. doi: 10.1093/cercor/bhm056.

Varga, V., B. Kocsis, and T. Sharp. 2003. "Electrophysiological Evidence for Convergence of Inputs from the Medial Prefrontal Cortex and Lateral Habenula on Single Neurons in the Dorsal Raphe Nucleus." *The European Journal of Neuroscience*

17(2):280–86.

Vints, Katlijn, Dorien Vandael, Pieter Baatsen, Benjamin Pavie, Frank Vernaillen, Nikky Corthout, Vasily Rybakin, Sebastian Munck, and Natalia V. Gounko. 2019. “Modernization of Golgi Staining Techniques for High-Resolution, 3-Dimensional Imaging of Individual Neurons.” *Scientific Reports* 9(1). doi: 10.1038/s41598-018-37377-x.

Wagner, Franziska, René Bernard, Christian Derst, Leon French, and Rüdiger W. Veh. 2016. “Microarray Analysis of Transcripts with Elevated Expressions in the Rat Medial or Lateral Habenula Suggest Fast GABAergic Excitation in the Medial Habenula and Habenular Involvement in the Regulation of Feeding and Energy Balance.” *Brain Structure and Function* 221(9):4663–89. doi: 10.1007/s00429-016-1195-z.

Walker, Ruth H., Gordon W. Arbuthnott, Robert W. Baughman, and Ann M. Graybiel. 1993. “Dendritic Domains of Medium Spiny Neurons in the Primate Striatum: Relationships to Striosomal Borders.” *The Journal of Comparative Neurology* 337(4):614–28. doi: 10.1002/cne.903370407.

Webster, Jack F., Rozan Vroman, Kira Balueva, Peer Wulff, Shuzo Sakata, and Christian Wozny. 2020. “Disentangling Neuronal Inhibition and Inhibitory Pathways in the Lateral Habenula.” *Scientific Reports* 10(1). doi: 10.1038/s41598-020-65349-7.

Weiss, T., and R. W. Veh. 2011. “Morphological and Electrophysiological Characteristics of Neurons within Identified Subnuclei of the Lateral Habenula in Rat Brain Slices.” *Neuroscience* 172:74–93. doi: 10.1016/j.neuroscience.2010.10.047.

Yang, Yan, Yihui Cui, Kangning Sang, Yiyan Dong, Zheyi Ni, Shuangshuang Ma, and Hailan Hu. 2018. “Ketamine Blocks Bursting in the Lateral Habenula to Rapidly Relieve Depression.” *Nature* 554(7692):317–22. doi: 10.1038/nature25509.

Yang, Yan, Hao Wang, Ji Hu, and Hailan Hu. 2018. “Lateral Habenula in the Pathophysiology of Depression.” *Current Opinion in Neurobiology* 48:90–96. doi: 10.1016/j.conb.2017.10.024.

Yizhar, Ofer, Lief E. Fenno, Thomas J. Davidson, Murtaza Mogri, and Karl Deisseroth. 2011. “Optogenetics in Neural Systems.” *Neuron* 71(1):9–34. doi: 10.1016/j.neuron.2011.06.004.

Zhang, Hai, Kuan Li, Hong-Sheng Chen, Shuang-Qi Gao, Zhi-Xuan Xia, Jie-Ting Zhang, Fang Wang, and Jian-Guo Chen. 2018. “Dorsal Raphe Projection Inhibits the Excitatory Inputs on Lateral Habenula and Alleviates Depressive Behaviors in Rats.” *Brain Structure and Function* 223(5):2243–58. doi: 10.1007/s00429-018-1623-3.

Zhang, Limei, and Vito S. Hernández. 2016. “Thirst Is Associated with Suppression of Habenula Output and Active Stress Coping: Is There a Role for a Non-Canonical Vasopressin-Glutamate Pathway?” 10(March). doi: 10.3389/fncir.2016.00013.

Zhang, Limei, Vito S. Hernández, Jerome D. Swinny, Anil K. Verma, Torsten Giesecke, Andrew C. Emery, Kerim Mutig, Luis M. Garcia-segura, and Lee E. Eiden. 2018. “A GABAergic Cell Type in the Lateral Habenula Links Hypothalamic Homeostatic and Midbrain Motivation Circuits with Sex Steroid Signaling.” *Translational Psychiatry*. doi: 10.1038/s41398-018-0099-5.

8 Affidavit / Eidesstattliche Versicherung

„Ich, Leo Fabig, versichere an Eides statt durch meine eigenhändige Unterschrift, dass ich die vorgelegte Dissertation mit dem Thema: „Electrophysiological and Morphological Characteristics of VGAT-YFP positive Neurons in the Lateral Habenula of the Rat“ selbstständig und ohne nicht offengelegte Hilfe Dritter verfasst und keine anderen als die angegebenen Quellen und Hilfsmittel genutzt habe.

Alle Stellen, die wörtlich oder dem Sinne nach auf Publikationen oder Vorträgen anderer Autoren beruhen, sind als solche in korrekter Zitierung kenntlich gemacht. Die Abschnitte zu Methodik (insbesondere praktische Arbeiten, Laborbestimmungen, statistische Aufarbeitung) und Resultaten (insbesondere Abbildungen, Graphiken und Tabellen) werden von mir verantwortet.

Meine Anteile an etwaigen Publikationen zu dieser Dissertation entsprechen denen, die in der untenstehenden gemeinsamen Erklärung mit dem Betreuer, angegeben sind. Für sämtliche im Rahmen der Dissertation entstandenen Publikationen wurden die Richtlinien des ICMJE (International Committee of Medical Journal Editors; www.icmje.og) zur Autorenschaft eingehalten. Ich erkläre ferner, dass mir die Satzung der Charité – Universitätsmedizin Berlin zur Sicherung Guter Wissenschaftlicher Praxis bekannt ist und ich mich zur Einhaltung dieser Satzung verpflichte.

Die Bedeutung dieser eidesstattlichen Versicherung und die strafrechtlichen Folgen einer unwahren eidesstattlichen Versicherung (§156,161 des Strafgesetzbuches) sind mir bekannt und bewusst.“

Datum: 14.04.2021

_____

Unterschrift des Doktoranden

9 Curriculum Vitae / Lebenslauf

Mein Lebenslauf wird aus datenschutzrechtlichen Gründen in der elektronischen Version meiner Arbeit nicht veröffentlicht.

10 Acknowledgements / Danksagung

Ich möchte mich zunächst bei meinem Doktorvater Prof. Imre Vida bedanken: Für seine immer offene Bürotür, seinen Scharfsinn und seine Genauigkeit. Er wird mir ein Vorbild sein, auch wenn ich einen anderen Weg einschlage.

Außerdem bedanke ich mich bei Anja Matthiä, die mir beim Experimentieren und Schreiben Struktur gegeben hat und auch aus der Schweiz noch zur Seite stand.

Ferner bin ich Ina Wolter, Paul Turko, Samuel Booker und Jie Song sehr dankbar, denn ohne ihr Wissen, der Bereitschaft es zu teilen und der guten Stimmung innerhalb der Arbeitsgruppe, hätte ich diese langen Jahre nicht überstanden.

Zuletzt möchte ich mich Erika Valle und Harald Lux einen großen Dank aussprechen. Sie sind mit gutem Beispiel vorangegangen, haben mich motiviert und keine Mühe gescheut, diese Arbeit von formalen Fehlern zu befreien. Ebenso danke ich meiner Familie, ohne die ich diesen Weg nicht hinter mich gebracht hätte.